Available online at www.sciencedirect.com
SCIENCE DIRECT®
Journal of Sound and Vibration 291 (2006) 566–603
JOURNAL OF SOUND AND VIBRATION
www.elsevier.com/locate/jsvi

Synchronization of two coupled escapement-driven pendulum clocks

M. Senator

Davidson Laboratory, Stevens Institute of Technology, Hoboken, NJ 07030, USA

Received 30 October 1998; received in revised form 6 June 2005; accepted 17 June 2005
Available online 2 September 2005

Abstract

The synchronization of two coupled, similarly sized, escapement-driven pendulum clocks is studied. These clocks are coupled by having their extended cases suspended from adjacent stiff beams that can move together horizontally. This setup models the system that Huygens studied in 1665, using clocks that he had designed for determining a ship's longitude. Huygens observed that the two clocks soon ran at a common rate, with the pendulums moving in opposition to each other. A quantitative approximate theory of this synchronization is developed herein. This theory explicitly includes the essential nonlinear elements of Huygens' system, which are the escapements, as well as the suspended-clock-case and non-identical-clock features of his setup.

1. Introduction

Synchronization of two or more coupled, similarly sized, nonlinear, autonomous oscillating systems occurs frequently, with many cases now being actively investigated. For instance, Mirollo and Strogatz [1] have analyzed a model that can represent the synchronized firings of the pacemaker cells that trigger heart beats. They also provide references to other studies of the synchronization of biological and mechanical oscillators.

Perhaps the earliest reports of the synchronization of two coupled, similarly sized, nonlinear, autonomous oscillating systems were by Huygens in 1665 [2,3]. Huygens observed that when two

E-mail address: msenator@stevens.edu.

0022-460X/$ - see front matter © 2005 Elsevier Ltd. All rights reserved.
doi:10.1016/j.jsv.2005.06.018

pendulum clocks designed for determining a ship's longitude were mounted with their extended cases suspended from stiff wooden beams that could move together horizontally, each clock soon adjusted its rate slightly to reach a common rate. The clocks then ran in a stable steady state at this common rate with their pendulums moving in opposition to each other.

In his communications to others Huygens limited himself to explaining synchronization by describing the setup (Fig. 1 shows Huygens' setup, a verge and crown wheel escapement, and an idealized model that incorporates essential features of this setup), noting the basic coupling mechanism, and describing how a steady state is approached. (Huygens originally thought the coupling was due to imperceptible air-borne forces transmitted between the pendulums of the two clocks [3], but within days he realized [4–7] that the coupling was due to structure-borne forces.) An embellishment of Huygens' published explanation follows. The common beam [6,7] or the two coupled beams [5] from which the extended clock cases are suspended can move horizontally, at least through small displacement amplitudes. The two pendulums, oscillating in the same or parallel planes, exert (through their pivots) oscillating forces on the two extended clock-cases, which, in turn, exert (through their pivots) oscillating forces on the beams. If the two pendulums are not started in opposition, the resultant oscillating force on the beams causes the beams to oscillate at imperceptibly small amplitudes. Because the two nearly identical clocks initially run at slightly different speeds their pendulums eventually get in opposition, the two oscillating force components almost completely cancel, and the motion of the beams goes to zero. Then the two clocks adjust their speeds, and their pendulums remain in opposition. So Huygens had noted two basic features of his setup—the clocks adjusting their speeds to a common speed (Huygens' two clocks, when running independently, differed by daily average times that ranged from $-1/2$ to 6 s. [4]); and the structure-borne nature of the coupling forces.

Korteweg [8] took the next steps in explaining Huygens' observations. Korteweg developed a dissipationless, three-degree-of-freedom, linear model that represents some features of Huygens' setup (this model is essentially equivalent to one formed from the five-degree-of-freedom model shown in Fig. 1 by clamping each extended clock-case to its support beam, removing all friction, and removing the escapements). Korteweg then observed how the natural frequencies and mode shapes of this model would vary as parameters vary, and used the study results to make informed guesses that explained the observed behavior of Huygens' real system. A paraphrase of Korteweg's basic idea follows. The stable, steady-state motions of the real, nonlinear, two-coupled-clock system can be approximately represented by his model vibrating in one of its normal modes at the corresponding natural frequency. The approximating mode/frequency pair is found by adding linear friction to the model, realistically assuming that pendulum friction is extremely small while beam-motion friction is (only) small, determining which of the three initial-condition-driven, exponentially-damped oscillating modes of the lightly damped linear model would persist the longest, and identifying the undamped normal mode that most closely approximates this persisting damped mode. Korteweg found that the undamped mode corresponding to the persisting damped mode would have a frequency between the frequencies of the two pendulums (oscillating independently from fixed pivots) and a mode shape with the pendulums moving in opposition to each other. So Korteweg added two basic ideas—that the actual nonlinear system's motion would be approximately like a modal motion of a related dissipationless linear system having similar inertial and stiffness properties; and that relative friction magnitudes would determine which mode would be the approximating one.

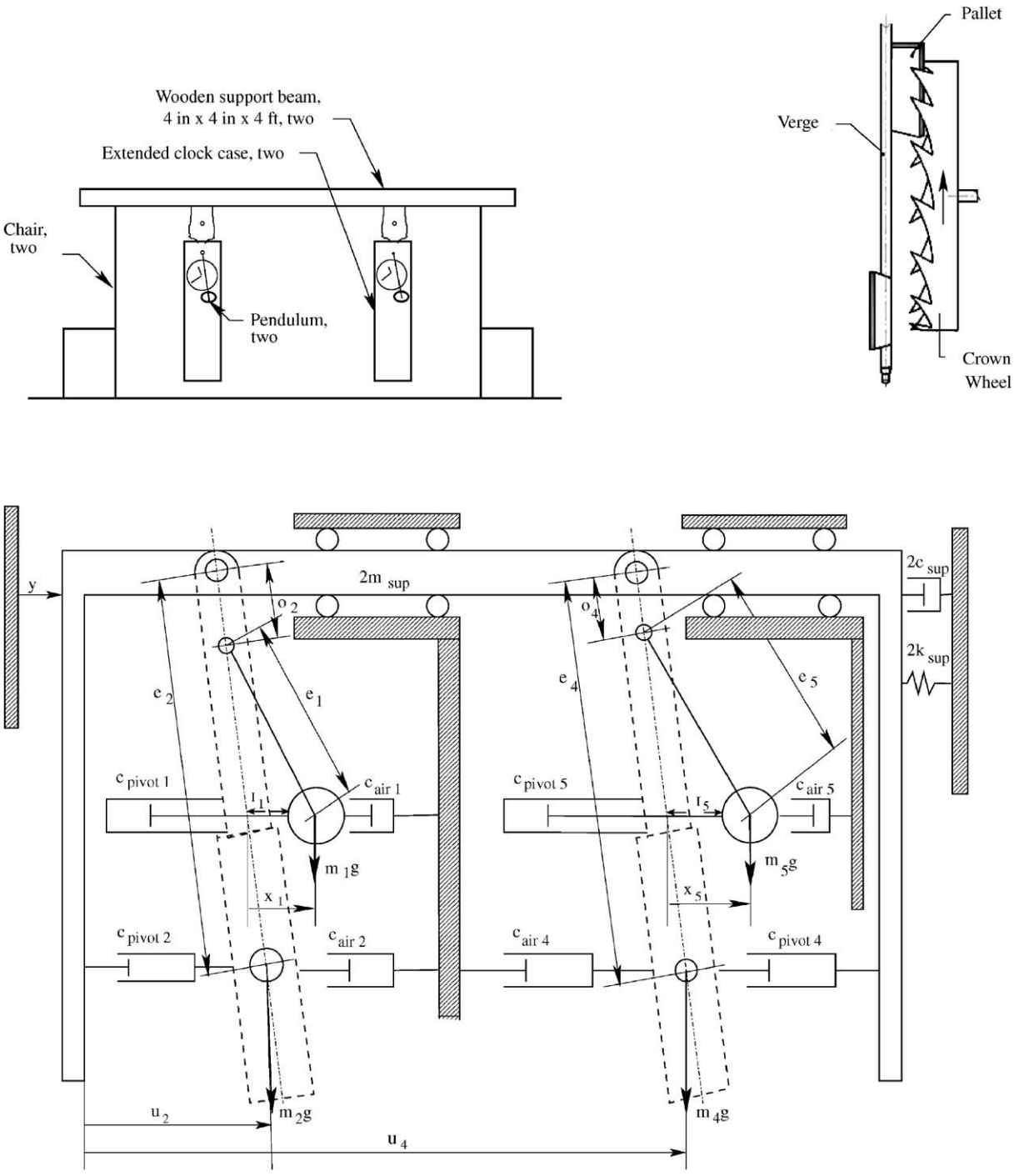

Fig. 1. Huygens' setup; a verge and crown wheel escapement; and the final, two-coupled-clock, sliding-support, suspended-clock-case, five degree-of-freedom model.

Recently the synchronization of Huygens-like systems has been studied by Blekhman [9], Bennett et al. [10], and Pantaleone [11]. These investigators have each tested three-degree-of-freedom two-clock systems that are coupled by the clock-cases being rigidly attached to a stiff common base that can move horizontally. Blekhman and Pantaleone have observed opposite-phase and same-phase synchronizations of the clocks' pendulums, while Bennett et al. have only observed opposite-phase synchronizations. Each has developed a theory that explains the synchronized motions they observed. Blekhman's and Pantaleone's theories use van der Pol-like terms to model the energy dissipation/resupply of the pendulums, while Bennett et al.'s theory uses a more realistic continuous dissipation/impulsive resupply model. Bennett et al.'s and Pantaleone's theories are for identical clocks, while Blekhman's considers the clocks to be identical to within the first power of the small parameter of the theory.

The immediate purpose of this study was to develop an intuitively clear approximate theory that would explain the observed synchronizations of two-clock systems. This theory would explicitly consider the essential nonlinearities of these systems, which are the impulsive firings of the escapements; explicitly allow for non-identical clocks; and explicitly include the suspended clock-case feature of Huygens' setup. It was found that the developed theory allows finding regions in parameter space for which one can predict, with high certainty, whether or not synchronization can occur. When synchronization is predicted, the theory allows determining the basic characteristics (approximate frequency, amplitudes, and relative phases) of the synchronized motions.

The basic method used is to extend Korteweg's idea of analyzing more tractable related systems. Thus, in addition to forming and analyzing related dissipationless- and damped-linear systems having the same inertial/stiffness/(damping) properties as the original nonlinear system, other related systems are also formed and analyzed. These include related dissipationless nonlinear systems having the same inertial/stiffness/escapement properties as the original systems, and related constrained single-degree-of-freedom nonlinear systems formed from the original systems by adding judiciously chosen rigid, massless, frictionless linear constraints. When the generalized constraining (reaction) forces/impulses of these systems are small, the necessarily proportional steady-state motions of these constrained systems are expected to accurately approximate the steady-state motions of the original intractable nonlinear systems.

In Section 2, the basic simplifications used to make the analyses tractable are discussed and some consequences of these simplifications are mentioned. In Section 3 a fixed-pivot idealized-escapement-driven pendulum clock model is analyzed exactly and approximately, and the exact and approximate analyses are compared. In Section 4, the fixed-pivot, one-clock model is modified by allowing the pendulum's pivot (the clock-case) to move horizontally. This change adds an essential feature of Huygens' setup to the model and allows developing an approximate technique for handling multi-degree-of-freedom models in a still-tractable, one-clock environment. The technique allows predicting essential characteristics of the stable, steady-state motions of one clock systems, and is calibrated by comparing the predicted approximate motions with numerically determined motions. In Section 5 the calibrated technique is applied to a two-coupled-clock, three-degree-of-freedom, sliding-clock-case model. Predictions are made for two-clock systems with parameters that could represent this simplified version of Huygens' setup. Huygens' (simplified) clocks are predicted to synchronize with the pendulums moving approximately in opposite phase, even when parameters are chosen that make the individual

average clock rates differ by more than 100 times the differences that Huygens measured. In Section 6, a five-degree-of-freedom, suspended-clock-case, two-clock model is developed, parameter values are chosen that reasonably represent Huygens' setup, and the developed technique is applied to this model. It is predicted that, as Huygens observed, the two clocks will synchronize with the pendulums moving nearly in opposite phase. The paper concludes by applying the technique to a version of the three-degree-of-freedom model of Huygens' setup for which absence of synchronization is predicted, by speculating as to what might actually occur when the theory predicts that the clocks will not synchronize, and by summarizing the results.

2. Basic simplifications

One simplification used here is to ignore all large pendulum amplitude effects. Thus, the angles between the pendulums and their vertical equilibrium positions and the rates of change of these angles are assumed to always remain small. The gravity force effects of this simplification on the intermediate amplitude oscillations of frictionless, fixed-pivot pendulums are well known and small: system trajectories go from a set of concentric ellipses traversed at a common rate to a set of concentric 'ovals' traversed at rates that decrease slowly as amplitude increases. Effects of this simplification also show up in the inertia force terms of the system equations when the pendulum pivots can move along horizontal lines. It is expected that, even with these additional effects, using the small amplitude simplification will allow meaningful predictions to be made.

A second simplification is to linearize all friction. This linear friction simplification captures two essential features of the actual friction: that at intermediate and high velocity amplitudes, friction forces increase as velocity magnitude increases, and, for suitably small friction parameter magnitudes, that cyclic energy dissipated is small compared to the energy that is cyclically converted between potential and kinetic forms. However, at low stored energy values this linear friction model does not capture the actual behavior of real clocks, where frictionally dissipated cyclic energy is not small compared to stored energy. Thus, all results here that have a pendulum pass through a low-energy cycle and continue running have to be examined critically. With this caveat, however, it is expected that using the linearized friction simplification will allow meaningful predictions to be made.

A third simplification has to do with modeling the nonlinear energy resupply feature of the escapement. Huygens' new pendulum-timed clocks used a then almost-400-year-old verge-and-crown-wheel escapement design (see Fig. 1). The oscillating angular motion of the pendulum is magnified using a forked crank and a pair of gears, so that the verge shaft oscillates (about a vertical axis, as shown) together with the pendulum. Falling weights, acting through pulleys and a gear train, drive the clock hands and the crown wheel. Then, at approximately opposite positions in the pendulum displacement cycle, opposite diameter crown-wheel teeth alternately impact the pallets, thereby providing energy to make up for energy dissipated by friction. It is customary to model the complex cyclic actions of this escapement on the driven, verge–gearing–linkage–pendulum assembly, and on the driving, weight–pulley–gear–train assembly, as impulses that act between two rigid bodies whenever pallet-to-tooth edge relative displacement becomes zero [12,10,14,15]. In particular, all between-impulse pallet-tooth (friction and normal) forces are assumed to have negligible effects on the dynamics of the pendulum. Thus, the

constant-impulse-magnitude escapement model of Andronov et al. [12] is adopted here. For this model, at two opposite points in the pendulum displacement cycle, a crown-wheel tooth hits a pallet (the escapement fires), and a constant magnitude impulse is applied between a rigid body having the effective inertia of the pendulum at the pitch radius of the impact, and a rigid body having the effective inertia of the driving train at the pitch radius of the impact. This model captures the impulsive energy resupply feature of the escapement in a straightforward way. The actual pair of firing phases used with this model does not affect the timing results of the analyses. For this reason, and because escapement firing when the pendulum passes through its equilibrium position allows using a clearer, intuition-guiding notation, the firing times of the model have been adjusted accordingly. It is expected that using this tractable model will give realistic results. However, the assumptions that an escapement fires during an exactly zero-length displacement interval and that any extremely small, but non-zero, impact velocity magnitude will allow escapement firing, are unrealistic. So, as with the linear friction simplification, all results that have a pendulum pass through a low-energy cycle and continue running have to be examined critically.

3. Fixed-pivot one-clock model

The fixed-pivot one-clock model is formed from the general model of Fig. 1 by considering only one clock, clamping its case to its support beam, and fixing the support beam in inertial space. The model reduces to a rigid body (the pendulum) pivoted from a fixed body (the clock-case-beam assembly) in a downward gravitational field. (Fig. 2, which does triple duty, represents the fixed-pivot one-clock model when y, the clock-case displacement coordinate, is constrained to be zero). Let x be the (small) horizontal displacement of the mass center of the pendulum, measured from a downward vertical line drawn on the clock case. Three parameters characterize the geometric and inertial properties of the model: m, the mass of the pendulum, e, the pendulum's length (the distance from its pivot to its mass center), and α, the square of the ratio of the pendulum's radius of gyration about its mass center to its length (inertial effects of the connected linkage, gear pair, and verge are included by increasing α so that total kinetic energy still equals $\frac{1}{2}m(1+\alpha)\dot{x}^2$). The resultant gravitational force on the pendulum has magnitude, mg, and acts downward through the mass center of the pendulum. Dissipation is modeled by two viscous dampers, both exerting horizontal retarding forces on the pendulum at its mass center. Pivot friction is modeled by a viscous damping coefficient, c_{pivot}, which multiplies the relative component of horizontal velocity, $\dot{x}$, while air resistance is modeled by a viscous damping coefficient, c_{air}, which multiplies the absolute component of horizontal velocity, which for this model is the same as the relative component. The idealized escapement acts whenever relative displacement, x, is zero and relative velocity, $\dot{x}$, is non-zero. At each of these instants the idealized escapement fires, imparting a horizontal impulse of fixed magnitude, I, between the pendulum and the clock-case at the level of the mass center of the pendulum, acting on the pendulum in the direction of its relative velocity, $\dot{x}$. Let t_j^+ be the time just after the jth firing of the escapement and $t_{j+1}^-$the time just before the $(j+1)$th firing of the escapement. Then, in the interval between two successive firings, $(t_j^+ < t < t_{j+1}^-)$, the relative displacement satisfies the linear, homogeneous differential equation

$$m(1+\alpha)\ddot{x} + (c_{\text{pivot}} + c_{\text{air}})\dot{x} + (mg/e)x = 0, \tag{1}$$

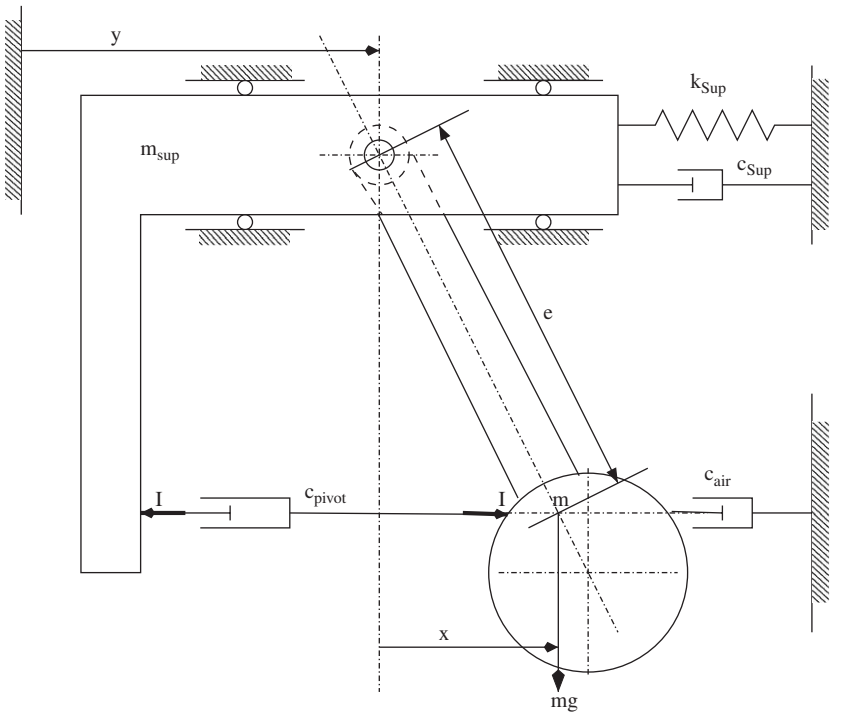

Fig. 2. Two idealized-escapement-driven one-clock models—fixed-pivot model with coordinate, y, constant; sliding-pivot model with coordinate, y, varying.

with initial conditions $x(t_j^+) = 0$ and $\dot{x}(t_j^+) \equiv v_j^+ \neq 0$. Eq. (1) must be satisfied until relative displacement, x, next becomes zero at t_{j+1}^- when the escapement fires. At the escapement firing instant the change in relative velocity, $\Delta\dot{x}_{j+1}$, must satisfy the impulse/momentum balance conditions (the change in linear momentum of a particle moving with the velocity of the mass center must equal the sum of the applied impulse and the impulsive pivot reaction, and the change in angular momentum about the mass center must equal the sum of the moments about the mass center of the applied impulse and the impulsive pivot reaction). Eliminating the impulsive pivot reaction from these conditions gives

$$m(1+\alpha)\Delta\dot{x}_{j+1} = I\,\mathrm{sign}(\dot{x}_{j+1}^-). \tag{2}$$

Introducing the notation

$$\begin{aligned}
&\omega_{\mathrm{n\,pend}} = \sqrt{[mg/e]/[m(1+\alpha)]}, \quad \omega_{\mathrm{decay\,pend}} = [c_{\mathrm{pivot}} + c_{\mathrm{air}}]/[2m(1+\alpha)],\\
&\gamma_{\mathrm{pend}} = \arcsin(\omega_{\mathrm{decay\,pend}}/\omega_{\mathrm{n\,pend}}), \quad \omega_{\mathrm{nd\,pend}} = \sqrt{\omega_{\mathrm{n\,pend}}^2 - \omega_{\mathrm{decay\,pend}}^2},\\
&T_{\mathrm{nd\,pend}} = 2\pi/\omega_{\mathrm{nd\,pend}}, \quad \Delta v = I/[m(1+\alpha)],
\end{aligned} \tag{3}$$

noting that γ_{pend} and $\omega_{\mathrm{nd\,pend}}$ are real since total pendulum friction is small; and treating x, $\dot{x}$, $\ddot{x}$, and $\Delta\dot{x}_{j+1}$ as one-component vectors, Eqs. (1,2) can be written in the generalizable forms

$$m(1+\alpha)\{\mathbf{M}_x\ddot{\mathbf{x}} + 2\omega_{\mathrm{n\,pend}}\sin\gamma_{\mathrm{pend}}\mathbf{C}_x\dot{\mathbf{x}} + \omega_{\mathrm{n\,pend}}^2\mathbf{K}_x\mathbf{x}\} = \{\mathbf{0}\}, \tag{4}$$

and

$$m(1+\alpha)\{\mathbf{M}_x\Delta\dot{\mathbf{x}}_{j+1}\} = I\{\mathbf{q}_x\}, \tag{5}$$

where $\mathbf{M}_x$, $\mathbf{C}_x$, and $\mathbf{K}_x$ are dimensionless, 1×1 inertia, damping, and stiffness matrices whose elements equal one; $\mathbf{q}_x$ is a one-component vector whose element equals $\text{sign}(\dot{x}_{j+1}^-)$; the scalar factors premultiplying $\mathbf{C}_x$ can also be written as $2\omega_{\text{decay pend}}$; and the time of the $(j+1)$th firing of the escapement, $t_{j+1}^- = (T_{\text{nd pend}}/2) + t_j^+$.

The phase-plane solution trajectory over the extended jth interval consists of two contiguous 'arcs'—the first a logarithmic spiral representing a half-cycle of an exponentially decaying oscillation with parametric equations

$$\begin{aligned} x(t-t_j^+) &= \frac{1}{\omega_{\text{n pend}}}\frac{v_j^+}{\cos\gamma_{\text{pend}}}\mathrm{e}^{-\omega_{\text{decay pend}}(t-t_j^+)}\cos(\omega_{\text{nd pend}}(t-t_j^+)-\pi/2),\\ \dot{x}(t-t_j^+) &= \frac{v_j^+}{\cos\gamma_{\text{pend}}}\mathrm{e}^{-\omega_{\text{decay pend}}(t-t_j^+)}\cos(\omega_{\text{nd pend}}(t-t_j^+)+\gamma_{\text{pend}}), \end{aligned} \tag{6}$$

and the second a radial line of signed length,

$$\Delta v\,\text{sign}(\dot{x}_{j+1}^-), \tag{7}$$

in the direction of the velocity axis representing the (constant displacement) impulsive change in velocity caused by the $(j+1)$th firing of the escapement.

The friction-caused velocity magnitude decrease during the jth oscillation half-cycle, $\Delta v_j \equiv |v_j^+| - |\dot{x}_{j+1}^-|$, is proportional to the magnitude of the initial velocity, $\Delta v_j = |v_j^+|(1-\mathrm{e}^{-\pi\tan\gamma_{\text{pend}}})$, while the escapement-firing-caused increase in velocity magnitude at the end of the interval is constant, equal to the value of the parameter, Δv. Thus, for high $|v_j^+|$, next interval starting velocity magnitude would decrease over the extended half-cycle, and for low $|v_j^+|$, next interval starting velocity magnitude would increase over the extended half-cycle. An intermediate value of $|v_j^+|$ must therefore exist such that next interval starting velocity magnitude equals $|v_j^+|$. Denoting this equilibrium velocity magnitude by v_P, we see that for this initial velocity the phase-plane trajectory closes.

It is straightforward to show that this closed trajectory is unique, and therefore forms a limit cycle [16,17]; that this limit cycle is stable, in that trajectories started outside or inside but not at the origin will asymptotically approach the limit cycle; and that the limit cycle peak velocity, v_P, and displacement amplitude, x_A, are given by

$$v_P = \left(\frac{\Delta v}{1-\mathrm{e}^{-\pi\tan\gamma_{\text{pend}}}}\right) = \omega_{\text{n pend}}\left(\frac{I}{c_{\text{pivot}}+c_{\text{air}}}\right)\left(\frac{2}{\pi}\right)\left(\frac{\pi\sin\gamma_{\text{pend}}}{1-\mathrm{e}^{-\pi\tan\gamma_{\text{pend}}}}\right) \tag{8}$$

and

$$\begin{aligned} x_A &= \left(\frac{\Delta v}{\omega_{\text{n pend}}}\right)\left(\frac{\mathrm{e}^{-(\pi/2-\gamma_{\text{pend}})\tan\gamma_{\text{pend}}}}{1-\mathrm{e}^{-\pi\tan\gamma_{\text{pend}}}}\right)\\ &= \left(\frac{I}{c_{\text{pivot}}+c_{\text{air}}}\right)\left(\frac{2}{\pi}\right)\left(\frac{\pi\sin\gamma_{\text{pend}}\mathrm{e}^{-(\pi/2-\gamma_{\text{pend}})\tan\gamma_{\text{pend}}}}{1-\mathrm{e}^{-\pi\tan\gamma_{\text{pend}}}}\right). \end{aligned} \tag{9}$$

These solutions show that the shape of the limit cycle, when made dimensionless and plotted with appropriate scales, is completely determined by the dimensionless friction parameter, γ_{pend}. Fig. 3 shows two limit cycle trajectories: one with $\sin\gamma_{\text{pend}} = 0.1$, a value large enough to show trajectory features clearly; and one with $\sin\gamma_{\text{pend}} = 0.005$, a realistic value of total pendulum friction for Huygens' clocks. Fig. 3 also shows about 3.4 half-cycles of a low-friction trajectory that starts outside of its limit cycle trajectory. For the higher damping value Fig. 3 clearly shows how the limit cycle trajectory spirals in for a half-cycle and then jumps outward when the escapement fires. For the more realistic lower damping value, however, one must look carefully to distinguish the actual trajectories from elliptical trajectories (circular trajectories for the original scales of Fig. 3) of a related dissipationless linear system that has the same inertial and stiffness properties as the actual system. In addition, at the realistic lower damping value, the oscillation frequency of the related dissipationless linear system, $\omega_{\text{n pend}}$, is an accurate approximation to the frequency of oscillation of the actual nonlinear system, $\omega_{\text{nd pend}}$.

To complete the approximation of the actual limit cycle trajectory, it is necessary to choose an amplitude for the trajectory of the related dissipationless linear system. This can be done using the first step of a conceptual iteration process: form a related damped linear system having the same inertial, stiffness, and damping parameters as the actual nonlinear system; constrain this related damped linear system to move as the related dissipationless linear system would over a half-cycle (harmonically); calculate the energy that would be dissipated during this constrained motion;

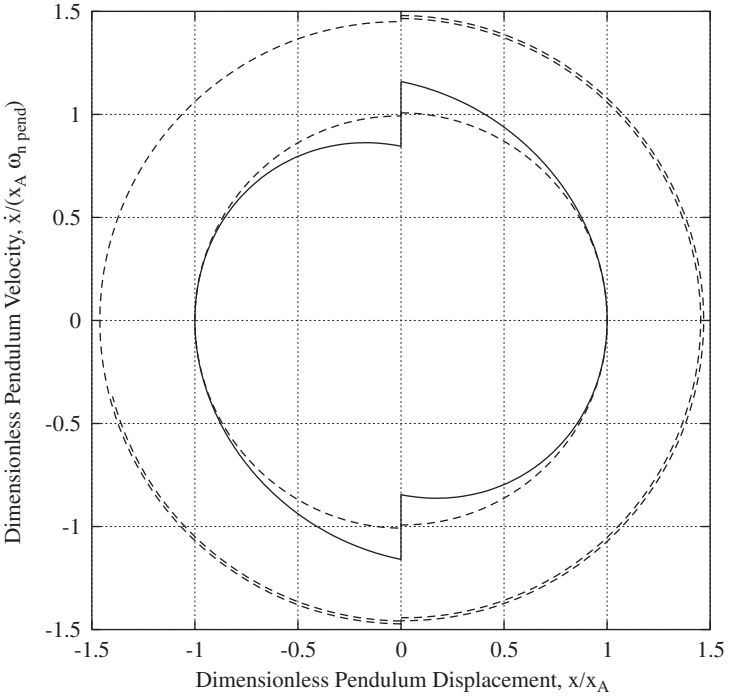

Fig. 3. Two steady-state limit cycle trajectories and one transient trajectory—solid curve, $\sin\gamma_{\text{pend}} = 0.1$; dashed curves, $\sin\gamma_{\text{pend}} = 0.005$.

equate this dissipated energy to the energy that would be imparted to the actual nonlinear system by the firing of the escapement when the pendulum has the peak velocity of the approximating motion; and solve the resulting equation for the peak velocity and displacement amplitudes of the approximating harmonic motion. The results of this first iteration are identical to the limiting forms of Eqs. (8,9) when the functions of γ_{pend} are expanded in powers of γ_{pend} and only the constant terms are retained (in the rightmost equalities the factors after the $2/\pi$ factors are replaced by their limiting values of one).

Note that for the original nonlinear system, or for any single-degree-of-freedom system (by the definition of a single-degree-of-freedom system), all mass points move together proportionally, reaching, for example, their maximum velocities simultaneously, and that this happens even though the points do not necessarily move harmonically. However, from the equations of the trajectories, Eqs. (6,7), and from Fig. 3, we see that for realistic values of total pendulum friction and over a small number of half-cycles, the mass points of the pendulum do move (together) nearly harmonically. This observation, and the success of the approximation using constrained motions, suggest that for multi-degree-of-freedom systems, useful approximations may be obtained by constraining these systems to move so that their trajectories project along a modal direction of the related dissipationless linear system. This idea is explored in the next section.

The exact and approximate analyses of the fixed-pivot, single-degree-of-freedom system can be summarized in the following generalizable way. If the system is started with, say, high-energy initial conditions, it will oscillate nearly harmonically at a frequency slightly less than the natural frequency of a related dissipationless linear system that has the same inertial and stiffness parameters. During any between impulse half-cycle of this oscillatory motion the exact phase-space trajectory will be accurately approximated by an elliptical trajectory of the related dissipationless linear system. Over many half-cycles friction and escapement firings will cause a gradual drift in trajectory amplitude, until an amplitude is reached at which the dissipated energy per half-cycle is balanced by the energy added by the firing of the escapement. Thus, the system will oscillate nearly harmonically with fundamental frequency and phase-plane trajectory shape largely determined by its inertial and stiffness properties and with initial amplitude largely determined by the initial conditions. Amplitude will gradually change over many cycles until a steady-state amplitude is reached that is largely determined by the system's damping and escapement properties.

4. Sliding-pivot, one-clock model

4.1. Model and equations

A sliding-pivot one-clock model is now formed from the fixed-pivot model by allowing the pivot to move horizontally. This new model is also shown in Fig. 2, with the supporting beam clock-case assembly now allowed to move. The sliding assembly forms a second rigid body of mass, m_{sup}, which moves horizontally with displacement coordinate, y, against a linear spring of stiffness, k_{sup}, and a linear damper of constant, c_{sup} (from Fig. 1 we see that this spring models the horizontal stiffness of the chair-backs, and this damper models the sum of the dissipations caused

by internal chair-back friction and by the air friction forces that act on the beam clock-case assembly).

Introduce six parameters as follows: corresponding to the x alone (y constrained to be zero, subscript pend) parameters defined in Eqs. (3), define a y alone (x constrained to be zero, subscript sup) frequency parameter, $\omega_{\text{n sup}}$, and a y alone decay rate parameter, $\omega_{\text{decay sup}}$; and define a structure-to-pendulum mass ratio parameter, μ, a structure-to-pendulum undamped natural frequency (stiffness) ratio parameter, f_{sp}, a structure-to-pendulum decay rate ratio parameter, f_{decay}, and a pendulum-air-damping-to-total-pendulum-damping ratio parameter, f_{air}, by

$$\begin{aligned}
&\omega_{\text{n sup}} = \sqrt{k_{\text{sup}}/(m + m_{\text{sup}})}, \quad \omega_{\text{decay sup}} = (c_{\text{sup}} + c_{\text{air}})/[2(m + m_{\text{sup}})],\\
&\mu = m_{\text{sup}}/m, \quad f_{\text{sp}} = \omega_{\text{n sup}}/\omega_{\text{n pend}}, \quad f_{\text{decay}} = \omega_{\text{decay sup}}/\omega_{\text{decay pend}},\\
&f_{\text{air}} = c_{\text{air}}/(c_{\text{air}} + c_{\text{pivot}}).
\end{aligned} \tag{10}$$

Then, denoting the coordinate vector for this system by $\mathbf{x} \equiv \begin{Bmatrix} x \\ y \end{Bmatrix}$, the system equations are given by Eqs. (4,5), where the matrices and the impulse forcing vector are now 2×2 and 2×1 and are given by

$$\begin{aligned}
&\mathbf{M}_x \equiv \begin{bmatrix} 1 & \dfrac{1}{1+\alpha} \\ \dfrac{1}{1+\alpha} & \dfrac{1+\mu}{1+\alpha} \end{bmatrix}, \quad \mathbf{C}_x \equiv \begin{bmatrix} 1 & f_{\text{air}} \\ f_{\text{air}} & \dfrac{1+\mu}{1+\alpha} f_{\text{decay}} \end{bmatrix}, \quad \mathbf{K}_x \equiv \begin{bmatrix} 1 & 0 \\ 0 & \dfrac{1+\mu}{1+\alpha} f_{\text{sp}}^2 \end{bmatrix},\\
&\{\mathbf{q}_x\} \equiv \begin{Bmatrix} \text{sign}(\dot{x}_{j+1}^-) \\ 0 \end{Bmatrix}.
\end{aligned} \tag{11}$$

4.2. Setting parameter values

Because intervals between successive firings of the escapement are no longer constant and given by a simple formula ($= T_{\text{nd}}/2$), numerical solutions of the system equations illustrate physical results more clearly then symbolic formulas would. Parameter values for these numerical solutions are chosen to represent pertinent features of Huygens' setup (as well as this simplified model allows).

The dimensionless inertial parameters are set at $\mu = 33$ and $\alpha = 0.01$. These choices represent the physical conditions that pendulum mass is small compared to support mass plus equivalent translating clock-case mass, and that pendulum mass is mostly that of the pendulum bob and is concentrated around the pendulums's mass center. It is expected that other inertia parameter choices that satisfy these physical conditions will give similar results.

There is virtually no information available for directly determining stiffness values for Huygens' setups (for example by calculating stiffnesses of the support chairs). Proceeding indirectly, the writer guessed that support natural frequency was low compared to pendulum natural frequency, with the greatest likely range of their ratio being ($0 < f_{\text{sp}} < 0.7$). The analyses of this section will show that the pertinent (clocklike) system behavior is insensitive to where in this range f_{sp} falls. So, for the straightforward two- and three-degree-of-freedom models of this and the following

section, the dimensionless stiffness parameter is arbitrarily set to $f_{\text{sp}} = 0.7$ to produce 'limiting' behavior; and for the more realistic five-degree-of-freedom models of Section 6 it is arbitrarily set to a 'most likely' value of $f_{\text{sp}} = 0.4$.

The dimensionless friction parameters are set to $\gamma_{\text{pend}} = \arcsin(0.005)$, $f_{\text{air}} = 0.5$, and $f_{\text{decay}} = 14$. This choice for total pendulum friction realistically represents the low friction of Huygens' clocks, and it is expected that other extremely low friction numerical choices will give similar results. The choice of the equal division of pendulum friction between its pivot- and air-friction parts represents a lack of knowledge about what this division might actually have been, and a judgment that, as long as both components are included, the particular value used for the parameter f_{air} will not significantly affect the results. The choice of $f_{\text{decay}} = 14$ corresponds, at the limiting stiffness parameter value of $f_{\text{sp}} = 0.7$, to a value of $\sin\gamma_{\text{sup}} \equiv \omega_{\text{decay sup}}/\omega_{\text{n sup}} = 0.1$ (it was decided to use f_{decay} rather than γ_{sup} as a dimensionless measure of support friction, since, as stiffness decreases through values in the realistic range and $\omega_{\text{decay sup}}$ remains constant, γ_{sup} increases and then is not defined). The numerical value chosen for the support friction parameter reflects the judgment that support (mostly chair-back) friction was large compared to total pendulum friction. It is expected that the particular value of support friction used will not significantly affect the results as long as support friction remains significantly greater than pendulum friction.

4.3. Related dissipationless linear system

The numerical analyses are started by analyzing the related dissipationless linear system, which is completely characterized by the values of the inertial and stiffness parameters. The squared undamped natural frequency ratios and the corresponding mode shapes are the characteristic numbers (eigenvalues) and characteristic vectors (eigenvectors) of the two matrix characteristic value problem,

$$(\omega^2_{\text{n}\,(k)}/\omega^2_{\text{n pend}})\mathbf{M}_x\mathbf{x}_{(k)} = \mathbf{K}_x\mathbf{x}_{(k)} \quad (\mathbf{x}_{(k)} = \{x_{(k)}, y_{(k)}\},\ k = 1, 2). \tag{12}$$

The characteristic values are non-negative and are distinct (for all parameter values that plausibly model Huygens' setup, namely $\mu > 0$, as it must be if the model is to have two-degrees-of-freedom, $\alpha \geqslant 0$, and $f^2_{\text{sp}} \geqslant 0$), and the two modal vectors are linearly independent. The modal vectors are orthogonal to each other with respect to both the inertia and stiffness matrices, $\mathbf{x}'_{(1)}\mathbf{M}_x\mathbf{x}_{(2)} = 0$ and $\mathbf{x}'_{(1)}\mathbf{K}_x\mathbf{x}_{(2)} = 0$, and are scaled (normalized) so that their first non-zero components are positive and their lengths with respect to the inertia matrix are one, $\mathbf{x}'_{(k)}\mathbf{M}_x\mathbf{x}_{(k)} = 1$.

Understanding the properties of the normal modes and frequencies of the related dissipationless linear system is a key to the physical understanding of the pendulum clock systems studied herein. Therefore, before considering exact numerical results, it is informative to see how simple, but accurate approximations to these results can be obtained, just by imposing the realistic physical conditions that support mass is significantly greater than pendulum mass ($\mu \gg 1$), pendulum mass is concentrated around the mass center of the pendulum ($\alpha \ll 1$), and the square of the ratio of support natural frequency to pendulum natural frequency is significantly less than one ($f^2_{\text{sp}} \ll 1$).

When the inertial and stiffness parameters satisfy these conditions, the individual modal motions of the related dissipationless linear system can each be accurately approximated by the motion of a (different) single-degree-of-freedom system formed by constraining the

two-degree-of-freedom system. The high-frequency modal motion (subscript (2)) can be accurately approximated by starting from an already encountered system, the one formed by constraining the support mass to be fixed (subscript pend). Correspondingly, the low-frequency modal motion (subscript (1)) can be accurately approximated by starting from another already encountered system, the one formed by constraining the pendulum to be fixed to the support mass (subscript sup). It is natural, therefore, to call the high-frequency mode/frequency pair 'clocklike', and the low-frequency one 'support-like', or 'non-clocklike'.

To develop an approximation to the clocklike mode/frequency pair, realistically assume that in this mode the small amplitude motion of the relatively massive support can initially be neglected. Thus start with the support mass being fixed (the fixed-pivot clock model). Then the pendulum would oscillate harmonically at $\omega_{\mathrm{n\,pend}}$. This motion would produce a harmonically varying horizontal component of the reaction force acting on the pivot with magnitude, $m\omega^2_{\mathrm{n\,pend}}\bar{x}$, where $\bar{x}$ is the relative displacement amplitude of the mass center of the pendulum. Next apply this force to the now-free-to-move support-mass/support-spring system. In the steady state this force would produce a harmonic support mass motion with amplitude, $\bar{y}$, that satisfies $\bar{y} = -\frac{\bar{x}}{(1+\mu)[\frac{\mu}{1+\mu}-f^2_{\mathrm{sp}}]}$. This easy to understand approximation straightforwardly explains essential features of the clocklike modal motion of the related dissipationless linear system. Features of the clocklike mode/frequency pair that we can immediately understand are that the undamped natural frequency is near that of the fixed-pivot clock; that all mass points move proportionally, with the support mass moving in opposition to the pendulum; that support mass amplitude is small compared to pendulum amplitude (being smallest when support spring stiffness is zero and approximately doubling but still remaining small when support spring stiffness is at its maximum likely value).

To develop a corresponding approximation to the non-clocklike mode/frequency pair, realistically assume that in this mode the relative-motion-caused horizontal component of the pivot reaction force exerted by the relatively low-mass pendulum on the support mass can initially be neglected. Thus start with the pendulum being fixed to the support mass. Then the support-mass/pendulum assembly would oscillate harmonically at the frequency, $\omega_{\mathrm{n\,sup}}$, with a displacement amplitude, $\bar{y}$. Next apply this harmonic displacement to the pivot of the now-free-to-pivot pendulum. In the steady state this applied harmonic pivot displacement would produce a harmonic relative pendulum motion with amplitude, $\bar{x}$, that satisfies $\bar{x} = \frac{\bar{y}f^2_{\mathrm{sp}}}{(1+\alpha)[1-f^2_{\mathrm{sp}}]}$. So again, an easy to understand approximation straightforwardly explains essential features of the non-clocklike modal motion of the related dissipationless linear system. Features of the non-clocklike mode/frequency pair that we can immediately understand are that the undamped natural frequency is near that of the constrained system formed by fixing the pendulum to the support mass; that all mass points move proportionally, with the pendulum moving in-phase with the support mass; and that pendulum amplitude, which is zero at the low stiffness limit and about equal to support amplitude at the high stiffness limit, depends strongly on the value of the support stiffness parameter.

Numerically calculated results support the immediate conclusions drawn from these approximate analyses and show additional features of the system. Fig. 4 shows, in a modified velocity plane (the axes, which are equally scaled, have the dimensions of length, so that lengths and angles in the plane have an intuitively clear meaning and displacements and velocities can be shown on the same plot), for $f_{\mathrm{sp}} = 0.7$, the normalized modal vectors, three equal energy

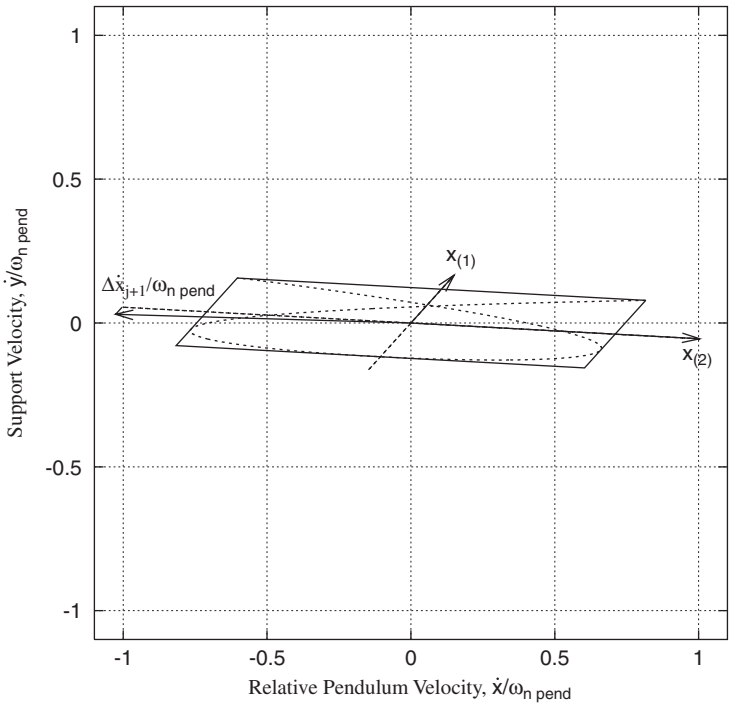

Fig. 4. Modified velocity plane for the stiffness parameter value, $f_{sp} = 0.7$—two normalized modal vectors (thick arrows); three equal energy trajectory projections (thick arrows/dashed lines and dashed curve); bounding parallelogram; and (large scaled) change in velocity vector (thin arrow).

trajectory projections, a bounding parallelogram for one of the trajectory projections, and a change in velocity vector. We see how essential features of the exact normalized modal vectors agree with those that can be inferred from the approximate analyses—the length of $\mathbf{x}_{(2)}$ is approximately equal to one and is significantly greater than the length of $\mathbf{x}_{(1)}$; $y_{(2)}$, the y component of $\mathbf{x}_{(2)}$, is small compared to $x_{(2)}$ and has the opposite sign; the length and direction of $\mathbf{x}_{(2)}$ are approximately independent of the value of the stiffness parameter (this only shows partially and indirectly in Fig. 4—the direction of $\mathbf{x}_{(2)}$ for zero stiffness is the negative of the direction of the change in velocity vector shown there); and $|y_{(1)}|$, while significantly less than $|x_{(2)}|$, still significantly exceeds $|y_{(2)}|$.

Two of the equal energy trajectories shown in Fig. 4 are modal trajectories, which have all of their energy in a normal mode of the related dissipationless linear system. The third trajectory has half of its energy in each normal mode. All three trajectory projections correspond to zero displacement initial conditions and non-zero velocity initial conditions. In a 'true' velocity plane the all-energy-in-the-low-frequency-mode trajectory projection would start at the tip of the $\omega_{\text{n pend}} \cdot \mathbf{x}_{(1)}$ vector, the all-energy-in-the-high-frequency-mode trajectory projection would start at the tip of the $\omega_{\text{n pend}} \cdot \mathbf{x}_{(2)}$ vector, and the half-energy-in-each-mode trajectory projection would start at the tip of the $(1/\sqrt{2})\omega_{\text{n pend}} \cdot (\mathbf{x}_{(1)} \mapsto \mathbf{x}_{(2)})$ vector (the upper right corner of the bounding parallelogram). The normalizing of the modal vectors to have unit lengths with respect to the $\mathbf{M}_x$

matrix assures that the two modal trajectories have equal energies, and the $(1/\sqrt{2})$ factor for the third trajectory assures that it has equal energy with half in each mode. In the modal trajectories all mass points (those on the pendulum and those on the support) move together proportionally (this shows up as the velocity and displacement plane trajectory projections always remaining on lines through the origin having the common slope of the modal vector) and harmonically (and therefore, periodically). Contrastingly, all mass points would not move together proportionally and harmonically for the half-energy-in-each-mode trajectory, even though the linearity of the system guarantees that this motion is the instantaneous sum of (equal fractions of) the two modal motions. However, Fig. 4 suggests that many observers might describe the velocity plane projection of the equal-energy-in-each-mode trajectory as showing a rapid, high velocity amplitude, primary oscillating motion in the clocklike modal direction with a superposed slow, low velocity amplitude, secondary oscillating (drifting) motion in the non-clocklike modal direction. These descriptions, and the arguments leading to the modal vector approximations and to the designations of these vectors as clocklike and non-clocklike, provide strong hints that the clocklike modal vector will play a controlling role in the following analyses.

4.4. Related dissipationless nonlinear system

The escapement is now added to the model and the resulting related dissipationless nonlinear system is analyzed. The formal analysis of the related dissipationless nonlinear system generalizes to higher-degree-of-freedom systems and introduces the normal coordinates subsequently used for the analyses of the related damped linear systems. But, before outlining the formal analysis, it is instructive to do an intuitively clear, but still exact analysis that is straightforward because this system has two-degrees-of-freedom. Since escapement firings only produce internal impulses on the system, and since the external horizontal force generating elements, the support spring and damper and the pendulum air resistance damper, cannot exert impulsive reactions on the system, the velocity of the mass center of the system does not change when the escapement fires. This restriction on mass center velocity change provides a necessary additional relation between the components of the change in velocity vector caused by the $(j+1)$th firing of the escapement: $\Delta\dot{y}_{j+1} = -\Delta\dot{x}_{j+1}/(1+\mu)$. The change in velocity vector (for negative before-firing pendulum relative velocity) is shown in Fig. 4 at a large scale, chosen so that this vector's projection along the clocklike modal direction equals the length of the normalized clocklike modal vector. At this scale Fig. 4 clearly shows that the firing of the escapement causes a significantly greater change in velocity in the direction of the clocklike modal vector (relative to the length of this vector) than in the direction of the non-clocklike modal vector (relative to the length of this vector). This significantly greater change in the clocklike modal velocity component translates directly to a significantly greater change in clocklike modal energy. So we see that escapement firing also favors the clocklike over the non-clocklike modal direction.

The formal analysis starts by symbolically solving the impulse/momentum balance equation, Eq. (5), for the change in velocity vector, $\boldsymbol{\Delta}\dot{\mathbf{x}}_{j+1}$. Towards this end, define a normalized modal matrix, $\mathbf{X}$, with columns equal to the normalized modal vectors in order of increasing frequency, $\mathbf{X} \equiv \left[\begin{Bmatrix} x_{(1)} \\ y_{(1)} \end{Bmatrix} \begin{Bmatrix} x_{(2)} \\ y_{(2)} \end{Bmatrix}\right]$, introduce normal coordinates, $\mathbf{w} \equiv \begin{Bmatrix} w_1 \\ w_2 \end{Bmatrix}$, by $\mathbf{x} \equiv \mathbf{X}\mathbf{w}$, substitute this definition

into the system equations, Eqs. (4,5), and premultiply the results by $\mathbf{X}'$, the transpose of the normalized modal matrix. In these normal coordinates the system equations are identical to Eqs. (4,5), with all appearances of x (in the variables and subscripts) replaced by w, and the matrices and forcing vector given by

$$\mathbf{M}_w = \begin{bmatrix} 1 & 0 \\ 0 & 1 \end{bmatrix}, \quad \mathbf{C}_w = \begin{bmatrix} \mathbf{x}'_{(1)}\mathbf{C}_x\mathbf{x}_{(1)} & \mathbf{x}'_{(1)}\mathbf{C}_x\mathbf{x}_{(2)} \\ \mathbf{x}'_{(2)}\mathbf{C}_x\mathbf{x}_{(1)} & \mathbf{x}'_{(2)}\mathbf{C}_x\mathbf{x}_{(2)} \end{bmatrix}, \quad \mathbf{K}_w = \begin{bmatrix} \dfrac{\omega^2_{\mathrm{n}\,(1)}}{\omega^2_{\mathrm{n\,pend}}} & 0 \\ 0 & \dfrac{\omega^2_{\mathrm{n}\,(2)}}{\omega^2_{\mathrm{n\,pend}}} \end{bmatrix},$$

$$\{\mathbf{q}_w\} = \mathrm{sign}(x_{(1)}\dot{w}^-_{1,j+1} + x_{(2)}\dot{w}^-_{2,j+1}) \begin{Bmatrix} x_{(1)} \\ x_{(2)} \end{Bmatrix}. \tag{13}$$

Because $\mathbf{M}_w$ is the 2×2 identity matrix, this change to the normal coordinates of the related dissipationless linear system has effectively solved the impulse/momentum balance equations. Note that, by the definition of the w-coordinates, the unit vectors, $\mathbf{w}_{(1)} \equiv \{{}^{1}_{0}\}$ and $\mathbf{w}_{(2)} \equiv \{{}^{0}_{1}\}$, respectively transform to the normalized x-coordinate modal vectors, $\mathbf{x}_{(1)}$ and $\mathbf{x}_{(2)}$. Thus, the solution of the impulse/momentum balance equations can be written directly in w-coordinates and then transformed to x-coordinates by premultiplying both sides by the normalized modal matrix. This gives

$$\Delta\dot{\mathbf{w}}_{j+1} = \frac{I}{m(1+\alpha)}\,\mathrm{sign}(x_{(1)}\dot{w}^-_{1,j+1} + x_{(2)}\dot{w}^-_{2,j+1})\{x_{(1)}\mathbf{w}_{(1)} + x_{(2)}\mathbf{w}_{(2)}\}, \tag{14}$$

which transforms to

$$\Delta\dot{\mathbf{x}}_{j+1} = \Delta v\,\mathrm{sign}(\dot{x}^-_{j+1})\{x_{(1)}\mathbf{x}_{(1)} + x_{(2)}\mathbf{x}_{(2)}\}.$$

Then, since $|x_{(2)}| \gg |x_{(1)}|$, we see formally that the change in velocity vector has a significantly greater relative component along $\mathbf{x}_{(2)}$ than along $\mathbf{x}_{(1)}$.

4.5. Related damped linear system

So far, analyses of an inertia/stiffness model and an inertia/stiffness/escapement model have indicated that these related systems favor the clocklike mode/frequency pair over the non-clocklike one. Now an inertia/stiffness/damping model, the related damped linear system, is analyzed. Because of the orthogonality of the modal vectors with respect to both the inertia and stiffness matrices, the w-coordinate inertia and stiffness matrices are diagonal. The w-coordinate damping matrix, however, can have non-zero off-diagonal elements, and these elements represent all the linear coupling of the system (note that the firings of the escapement also weakly, and nonlinearly, couple the w-coordinate equations of the original nonlinear system). Before examining effects of the linear coupling in more detail, it is useful to consider a simpler, (more distantly) related, w-coordinate-defined, *uncoupled* damped linear system. In w-coordinates this related uncoupled damped linear system has the elements of its inertia and stiffness matrices and the diagonal elements of its damping matrix equal to those of the related (coupled) damped linear system (see Eqs. (13)); however, the off-diagonal elements of its damping matrix are zero.

Analyzing the related uncoupled damped linear system allows us to understand, without the distractions produced by the coupling, a basic feature of the related damped linear system—that if modal decay rates are significantly different from each other, then one damped mode will persist after the other has effectively decayed to zero.

Start, by analogy with the definitions of the constrained decay rates, $\omega_{\text{decay pend}}$ and $\omega_{\text{decay sup}}$, by defining modal and coupling decay rates, $\omega_{\text{decay}\,(k)} \equiv \omega_{\text{decay pend}} \cdot \mathbf{C}_w(k,k)$ and $\omega_{\text{decay}\,(1,2)} \equiv \omega_{\text{decay pend}} \cdot \mathbf{C}_w(1,2)$ (in general the subscripts (k) and (i,j) are used to denote the diagonal and off-diagonal elements of the w coordinate modal and coupling decay rates). Then, observe from Eqs. (4,11,13) that the dominating parts of the diagonal terms of the $\mathbf{C}_w$ matrix arise from the large magnitude $\frac{1+\mu}{1+\alpha} f_{\text{decay}}$ term of the $\mathbf{C}_x$ matrix being multiplied by the squares of the y-components of the normalized modal vectors. Because the square of the y-component of the non-clocklike modal vector is significantly greater than that of the clocklike modal vector, the non-clocklike mode's decay rate is significantly greater than that of the clocklike mode (for this example about 5.5 times greater). We can see effects of this large difference in decay rates by returning to Fig. 4 and imagining what three equal initial energy trajectories of the related uncoupled damped linear system would look like. The two damped modal trajectories would again start at the tips of the modal vectors and the equal-initial-energy-in-each-mode trajectory at the upper right corner of the parallelogram. Now the modal trajectory projections would represent exponentially decaying damped oscillations with damped modal natural frequencies, $\omega_{\text{nd}\,(k)}$, that are slightly less than the corresponding undamped modal natural frequencies, $\omega_{\text{n}\,(k)}$. In these damped modal motions the mass points of the system would no longer move harmonically (or periodically), but the mass points would still move together proportionally, reaching, for example, zero displacement simultaneously. The damped modal trajectories would still lie in the directions of the modal vectors of the related dissipationless linear system, but would now decay, with the non-clocklike mode decaying more rapidly than the clocklike mode.The damped equal-initial-energy-in-each-mode trajectory would start by looking like a lightly damped version of the trajectory pictured in Fig. 4. However, the bounding parallelogram, instead of being fixed, would now have sides that shrink, with the sides parallel to the non-clocklike modal vector shrinking about 5.5 times more rapidly than the initially longer sides parallel to the clocklike modal vector. The result would be that after, say, five time constants of the more rapidly decaying motion $(5/\omega_{\text{decay}\,(1)})$, the decaying oscillating motion that started out with equal energy in each mode would have practically all of its energy in the clocklike mode. The clocklike mode would persist after the non-clocklike mode has disappeared. So, uncoupled damping clearly favors the clocklike mode/frequency pair over the non-clocklike one, and this favoring ultimately comes about mainly because support mass is significantly greater than pendulum mass and support friction is significantly greater than pendulum friction.

Including coupling in the analysis of the related damped linear system shows essentially the same result, that the clocklike damped mode would persist after the non-clocklike one has decayed. The analysis also shows that for a damped modal motion the mass points of the system no longer move exactly proportionally but only approximately proportionally. Because all friction is small, the decay rates and damped natural frequencies of the coupled model (the real and imaginary parts of the complex-valued characteristic numbers, $-\omega_{\text{decay}\,[k]} \pm \text{i}\omega_{\text{nd}\,[k]}$) would be approximately equal to those calculated for the uncoupled model (subscript (k)). These results are illustrated in Fig. 5. There, equal initial energy velocity plane trajectory projections analogous to

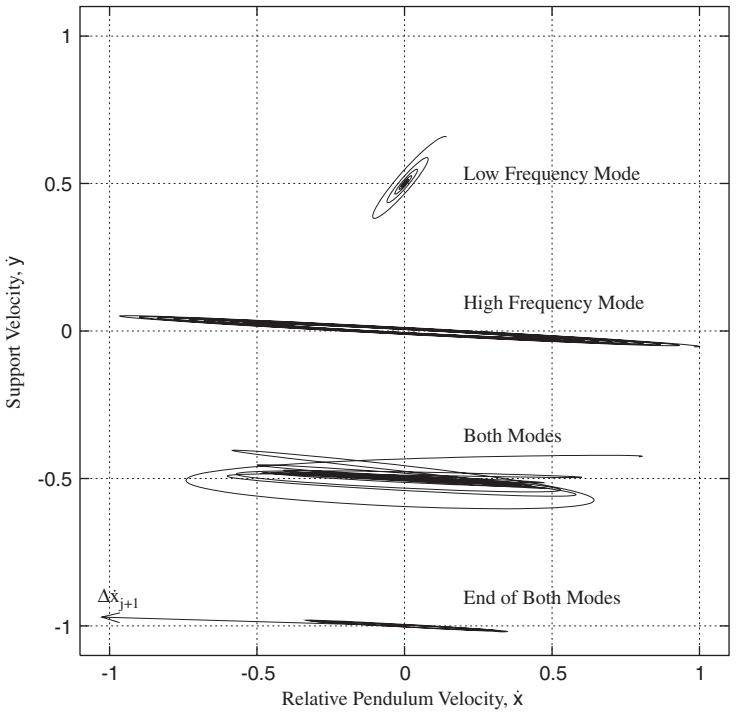

Fig. 5. Three equal initial energy damped modal motions: top curve—all initial energy in the damped, non-clocklike, low-frequency mode; second curve—all initial energy in the damped, clocklike, high-frequency mode; third curve—half initial energy in each damped mode; bottom curve—half initial energy in each damped mode after four time constants of the damped, non-clocklike mode; also a (large scaled) change in velocity vector.

those of Fig. 4 are shown. The trajectories are shown offset from each other for clarity—each trajectory is actually centered about the zero ordinate value. The upper curve shows the trajectory projection of the all initial energy in the damped non-clocklike (low frequency) mode case, the second curve shows the trajectory projection of the all initial energy in the damped clocklike (high frequency) mode case, and the third and fourth curves show the trajectory projection of the half initial energy in each damped mode case. The first three curves are drawn over an interval corresponding to five time constants of the most rapidly damped (the low frequency) mode, $(0<t<5/\omega_{\text{decay}\,[1]})$, while the fourth curve is drawn over the last fifth of this interval.

Instead of the exactly proportional damped modal motions of the related uncoupled damped linear system, we see nearly proportional damped motions. The nearly proportional nature of the motions shows up, for example on the top curve, as the inwardly spiraling trajectory projection lying near the line through the origin that has the direction of the low-frequency modal vector rather than lying exactly on it. Instead of the pendulum relative velocity and the support velocity reaching their minimum values simultaneously, as they would in a proportional motion, we see a small lag, with the pendulum reaching its minimum velocity (at the vertical tangent to the left of the outer loop of the spiral) slightly before the support mass reaches its minimum velocity (at the horizontal tangent below the outer loop of the spiral). A similar result holds for the clocklike mode. Again the motion is nearly proportional rather than exactly proportional, with the spiral

lying near the modal direction rather than directly along it. And similarly, instead of the pendulum relative velocity and the support velocity reaching opposite extreme values simultaneously, as they would in the corresponding proportional motion, the support mass achieves its maximum velocity (at the horizontal tangent above the outer loop of the spiral) slightly before the pendulum achieves its minimum velocity (at the vertical tangent to the left of the outer loop of the spiral). Note that the clocklike damped modal motion is more nearly proportional than the non-clocklike one, as its longer spiral is narrower than that of the non-clocklike motion. The half-initial-energy-in-each-damped mode trajectory shows effects of the different decay rates and initial amplitudes. We can recognize the first three left-right-left swings of this trajectory as a lightly damped version of the corresponding undamped trajectory of Fig. 4, before the swings of this damped trajectory smear together. The basic result is apparent on the bottom curve. We see that after the more heavily damped, smaller initial amplitude, non-clocklike mode has effectively decayed to zero, the trajectory has now become a lower-energy version of the all-energy-in-the-damped-clocklike mode trajectory. A change in velocity vector is also superposed on the bottom trajectory to show how the (mean) direction of the persisting damped mode and the direction of the change in velocity vector almost coincide but are distinct (these directions coincide at the zero-stiffness-parameter limit). So we see that for the related damped linear system, the clocklike mode is again favored over the non-clocklike one, the immediate reason being that the modal decay rate of the clocklike mode (as measured approximately by $\omega_{\text{decay}\,(2)}$ or exactly by $\omega_{\text{decay}\,[2]}$) is significantly less than that of the non-clocklike mode.

4.6. Related constrained single-degree-of-freedom systems

Next consider a set of related, constrained, single-degree-of-freedom nonlinear systems that have the same inertial, stiffness, dissipational, and escapement properties as the original two-degree-of-freedom nonlinear system. We can understand the basic features of these constrained systems by considering a modal motion of the related dissipationless linear system. For such a motion, where all mass points of the system move together proportionally, the point on the (possibly extended) centerline of the pendulum (the line on the pendulum from its pivot to its mass center) at a signed distance below the pivot of $d_{(k)} \equiv -(y_{(k)}/x_{(k)}) \cdot e$ has identically zero horizontal displacement. If a small, massless rigid pin were pressed into the pendulum at this point with its projecting end moving without friction between vertical guides, the modal motion of the related dissipationless linear system would not change, and the system would continue to move with zero constraining (reaction) forces exerted on the pin by the guides. Now imagine that a similar rigid, massless, frictionless constraining pin were placed anywhere along the (possibly extended) centerline of the pendulum of the actual nonlinear two-degree-of-freedom system. This linear constraint (linear between the coordinates, x and y) would reduce the system to a nonlinear single-degree-of-freedom system with all mass points constrained to move proportionally. The dynamic properties of the constrained system would be closely related to those of the unconstrained system. The important basic difference would be that the guides would now be able to exert reaction forces and impulses on the system. From the previous analyses we might expect that such a constraint, forcing the original system to move proportionally, with velocity- and displacement-plane trajectory directions corresponding to the clocklike modal direction of the related

dissipationless linear system, would allow constrained motions that are accurate approximations to the motions of the actual nonlinear system.

Each pin location determines a different constrained system, and corresponds to a direction in the x, y coordinate, velocity- and displacement-subspaces. The direction of the clocklike modal vector of the related dissipationless linear system is of most interest for two reasons. First, the firing of the escapement causes a change in velocity vector that departs only slightly from this clocklike modal direction (see Figs. 4, 5). Thus, constraining the system so that the trajectory projections lie in this direction produces what one hopes will be relatively small escapement-firing-associated errors. And second, the persisting (clocklike) modal trajectory of the related damped linear system lies, on the average, in this direction, so that constraining the trajectories to this direction would again produce what one hopes will be relatively small dissipation-associated errors.

Each constraining direction and the differential- and impulse/momentum balance equations of the two-degree-of-freedom nonlinear system determine the differential- and impulse/momentum balance equations of a related constrained single-degree-of-freedom system. These constrained equations are similar to the equations of the fixed pivot clock (with different coordinates and different parameter values), and the solutions of Section 3 apply. So all characteristics of the steady-state motion of the constrained system can be determined. Because a one-clock system has only one escapement, computational problems associated with the system equations being stiff [18,19] (the intervals between the firings of different escapements can be small compared to the intervals between successive firings of individual escapements) do not arise. Thus a steady-state solution of the nonlinear system equations can be found numerically and compared to the approximate solutions corresponding to different constraining directions. Fig. 6 shows such a

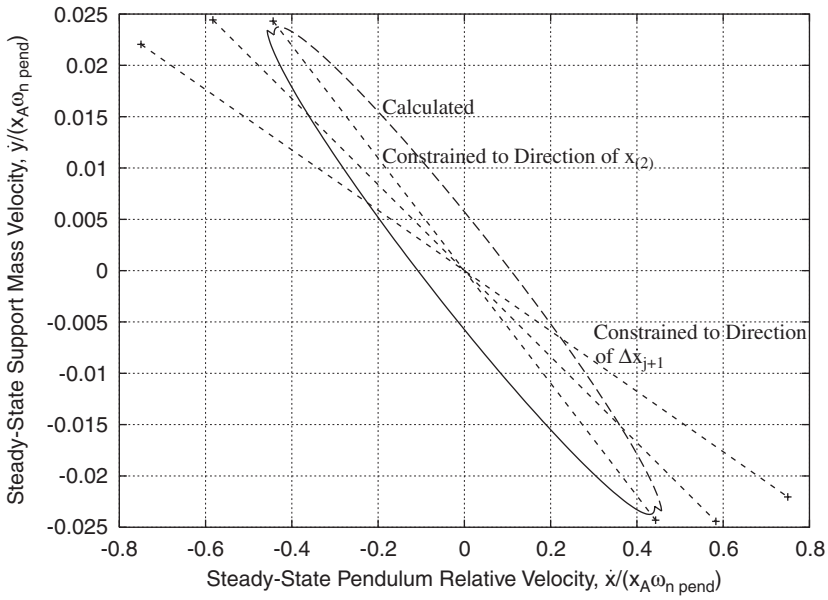

Fig. 6. Calculated and constrained velocity plane trajectory projections.

comparison. It shows an exact, numerically calculated steady-state velocity plane trajectory projection and compares it to three constrained system trajectory projections: one in the direction of the clocklike modal vector, one in the neighboring direction of the change in velocity vector, and one half-way between these two. Note that unlike Figs. 3–5, the ordinate and abscissa scales are not equal in Fig. 6—the ordinate scale is magnified so that the range of ordinate values is only 1/32 that of abscissa values. We see how the easily calculated characterizing features of the steady-state motion of the modally constrained single-degree-of-freedom system accurately approximate the corresponding features of the exact system. For example, the exact pendulum velocity amplitude, the rightmost extreme abscissa value along the calculated curve (at the outer end of the line segment representing an escapement-firing-caused change in velocity), is accurately approximated by the abscissa of the '+' symbol that represents the steady-state pendulum velocity amplitude of the modally constrained system. We also see how sensitive the accuracy of this approximation is to the constraint direction in the velocity- and displacement-planes being exactly in the direction of the (clocklike) modal vector of the related dissipationless linear system—small departures from the exact direction produce relatively large errors in amplitude.

An important difference between the steady-state motions of the sliding- and fixed-pivot clocks should be noted. Constraining the sliding pivot system to the direction of the x-axis[1] produces a dimensionless velocity amplitude that is slightly greater than one (see the maximum ordinate value of the lower damping trajectory of Fig. 3). However, small departures from this preferred constraining direction produce large decreases in steady-state pendulum velocity amplitude. For example, the small direction changes to the directions of the $\Delta\dot{\mathbf{x}}_{j+1}$ and $\mathbf{x}_{(2)}$ vectors reduce the pendulum velocity amplitudes to about 0.75 and 0.44. Because support friction is significantly greater than pendulum friction, even small support mass amplitudes (small angles with the x-axis in the velocity- and displacement-planes) cause significant reductions in pendulum amplitudes. In a practical sense then, the fixed-pivot clock is optimum, in that its motion does not waste any escapement-supplied energy in moving the support mass against the relatively high support friction. We should also make a reality check here. We have to decide whether this model, with added threshold friction and finite escapement limits would, for a clock designed for a fixed-pivot pendulum velocity amplitude of 1.0, have a threshold restarting velocity amplitude that is significantly less than 0.44. The writer guesses that this would happen, so that the predicted motions could actually occur.

4.7. Application to two-clock systems

The agreement of the approximate and exact analyses of this one-clock system leads us to expect that similar approximate analyses could give accurate approximations to the synchronized steady-state motions of two-clock systems. For example, suppose a two-clock system were started with high-energy initial conditions. Further, suppose that this system has a clocklike mode/frequency pair with a decay rate that is significantly less than the smallest decay rate of the remaining mode/frequency pairs. Then, while the stored energy remains high, the cyclic energy supplied by the escapements would be small compared to the cyclic energy dissipated in friction,

[1]This simplified language is used to concisely, if imprecisely, express the idea that the direction of the trajectory projections in the velocity- and displacement-subspaces is in the direction of the x-axis.

and the system would almost oscillate the way its related damped linear system would. After a while the motion would become a slightly perturbed (by the escapement firings) version of the persisting motion of the related damped linear system. Since this motion would be approximately proportional, the zero displacement times of the two pendulums would be nearly simultaneous, and the two escapements would fire nearly simultaneously, in the directions (same or opposite) determined by the modal direction corresponding to the favored, lowest-decay-rate mode. If these nearly simultaneous firings would put significantly more energy into the damping-favored mode than into any other mode, we would then expect that the pendulums would synchronize, moving in the steady state in a way similar to the way the single-degree-of-freedom system formed by constraining the two-clock system to move in the favored modal direction would move. We would, therefore, expect this two-clock system to synchronize, with its steady-state synchronized motions accurately approximated by the steady-state motions of the appropriate related modally constrained single-degree-of-freedom system. This technique is applied in the following sections.

5. Two-coupled-clock, sliding-pivot, three-degree-of-freedom model

5.1. Model and equations

We now analyze a straightforward two-coupled-clock system—the system formed by clamping the support beams of two sliding-pivot, side-by-side, one-clock models of Fig. 2 together (this system can also be visualized as being formed from the five-degree-of-freedom model of Fig. 1 by clamping the clock cases to their already clamped-to-each-other support beams). This two-clock system is closely related to the one-clock systems that form its parts. However, the analyses will show that the steady-state behavior of this two-clock system can be significantly different. Even though the non-clocklike- and one clocklike-mode/frequency pair of the related dissipationless linear system of the two-clock system are straightforward generalizations of those of the one-clock system, the additional, also clocklike, mode/frequency pair is the one that would typically be associated with an approximating synchronized steady-state solution.

To have the notation reflect the connectivity of this system, the individual clocks are given the subscripts 1 and 3, and the coordinate vector is denoted by $\mathbf{x} \equiv \{x_1, y, x_3\}$. The system is described by 16 parameters: six for each clock, m_i, α_i, $c_{\text{pivot}\,i}$, $c_{\text{air}\,i}$, e_i, and I_i $(i = 1, 3)$; the gravitational acceleration, g; and three support parameters, $2m_{\text{sup}}$, $2c_{\text{sup}}$, and $2k_{\text{sup}}$. The system equations can be written in an intuitively clear form if redundant notation is introduced. Thus, the clocks are also described by six non-subscripted average parameters and six dimensionless (normally small) half-difference parameters defined by six pairs of equations like $m \equiv (m_1 + m_3)/2$ and $\varepsilon_m \equiv (m_1 - m_3)/(2m)$. The matrices and the impulse forcing vector for this two clock system can then be written as

$$\mathbf{M}_x \equiv \frac{1}{m(1+\alpha)} \begin{bmatrix} m_1(1+\alpha_1) & m_1 & 0 \\ m_1 & m_1 + 2m_{\text{sup}} + m_3 & m_3 \\ 0 & m_3 & m_3(1+\alpha_3) \end{bmatrix},$$

$$\mathbf{C}_x \equiv \frac{1}{c_{\text{pivot}} + c_{\text{air}}} \begin{bmatrix} c_{\text{pivot 1}} + c_{\text{air 1}} & c_{\text{air 1}} & 0 \\ c_{\text{air 1}} & c_{\text{air 1}} + 2c_{\text{sup}} + c_{\text{air 3}} & c_{\text{air 3}} \\ 0 & c_{\text{air 3}} & c_{\text{pivot 3}} + c_{\text{air 3}} \end{bmatrix},$$

$$\mathbf{K}_x \equiv \frac{1}{mg/e} \begin{bmatrix} m_1 g/e_1 & 0 & 0 \\ 0 & 2k_{\text{sup}} & 0 \\ 0 & 0 & m_3 g/e_3 \end{bmatrix}, \quad \{\mathbf{q}_x\} \equiv \frac{1}{I} \begin{Bmatrix} I_1 \operatorname{sign}(\dot{x}^-_{1,j+1}) \\ 0 \\ I_3 \operatorname{sign}(\dot{x}^-_{3,j+1}) \end{Bmatrix}, \tag{15}$$

where, to simplify notation, it is understood that if only escapement 1 fires, I_3 is to be set to zero; if only escapement 3 fires, I_1 is to be set to zero; and if both escapements fire simultaneously, the impulse forcing vector is to be used as written.

5.2. Setting parameter values

Numerical results are calculated for two manifestations of this model—an identical-clock manifestation and a similar-clock manifestation with small, but non-zero half-difference parameters. The average parameter values for both manifestations are made equal to each other and are chosen to be the same as the parameters of the one-clock model of the previous section. The half-difference parameters for the different-clock manifestation were chosen as follows. First, a reference half-difference pendulum length parameter, $\varepsilon_{\text{e ref}}$, is calculated by $\varepsilon_{\text{e ref}} \equiv 6/(24 \cdot 3600) \approx 0.00007$. For as realistic a model of Huygens' setup as this three-degree-of-freedom model allows, this value of ε_{e} would make effects of pendulum length alone cause Huygens' two, nominal-one-second-period [13] clocks to have fixed-pivot undamped natural frequencies that correspond to about a 6 s difference per day, the maximum difference that Huygens observed with his clocks running independently [4]. To clearly show effects of having similar, but unequal, clock parameter values, the magnitude of the difference between the pendulum lengths of Huygens' clocks was exaggerated. The algebraic signs of the half-difference parameters were also chosen so that all parameters act in the same direction, the direction that makes clock 1 more sluggish. Thus an exaggerated value of ε_{e} over 100 times greater than $\varepsilon_{\text{e ref}}$, and arbitrary but still reasonably small values for the other five ε's were chosen: $\varepsilon_{\text{e}} = +0.008$, $\varepsilon_m = +0.004$, $\varepsilon_\alpha = +0.10$, $\varepsilon_{c_{\text{pivot}}} = +0.08$, $\varepsilon_{c_{\text{air}}} = +0.08$, and $\varepsilon_I = -0.12$.

5.3. Results

Analysis results for these manifestations are shown in Table 1—rows 1–6 show the undamped natural frequencies and modal vectors of the related dissipationless linear systems (the modal vectors are normalized here by $\mathbf{x}'_{(k)}\mathbf{M}_x\mathbf{x}_{(k)} = 2$ to facilitate comparisons with those of the one-clock system); rows 7–10 show the change in velocity vectors; rows 11–14 show the modal- and coupling-decay rates for the related damped linear system; and rows 15–17 show the normalized velocity amplitude components for the modally constrained single-degree-of-freedom systems (subscripts $\{k\}$).

Consider the identical clock manifestation first. If we temporarily unclamp the support beams and start each of the resulting one-clock systems with identical initial conditions, the two systems

Table 1
Comparing two, three-degree-of-freedom, two-clock, sliding-pivot systems

Row	Item	Symbol	Identical clocks	Clock 1 sluggish
1	Natural frequency,	$\omega_{n\,(1)}/\omega_{\text{n pend}}$,	0.690874,	0.690873,
2	modal vector	$\mathbf{x}_{(1)}$	{0.15012, 0.16604, 0.15012}	{0.15258, 0.16604, 0.14771}
3		$\omega_{n\,(2)}/\omega_{\text{n pend}}$,	1.0,	0.999358,
4		$\mathbf{x}_{(2)}$	{1.0, 0, −1.0}	{1.13639, −0.00878, −0.84011}
5		$\omega_{n\,(3)}/\omega_{\text{n pend}}$,	1.028292,	1.028988,
6		$\mathbf{x}_{(3)}$	{1.00372, −0.05502, 1.00372}	{0.83984, −0.05385, 1.14563}
7	Change in	$\Delta\dot{\mathbf{w}}_{j+1\text{ esc 1 only}}/\Delta v$	{0.10615, 0.70711, 0.70974}	{0.09494, 0.70712, 0.52259}
8	velocity vectors	$\Delta\dot{\mathbf{w}}_{j+1\text{ esc 3 only}}/\Delta v$	{0.10615, −0.70711, 0.70974}	{0.11698, −0.66533, 0.90730}
9		$\Delta\dot{\mathbf{w}}_{j+1\text{ same dir}}/\Delta v$	{0.21231, 0, 1.41948}	{0.21192, 0.04179, 1.42989}
10		$\Delta\dot{\mathbf{w}}_{j+1\text{ opp dir}}/\Delta v$	{0, 1.41421, 0}	{−0.02204, 1.37246, −0.38470}
11	Modal and		13.04 0 −4.08	13.04 0.63 −4.03
12	coupling	$\omega_{\text{decay }(i,j)}/\omega_{\text{decay pend}}$	0 1.0 0	0.63 1.06 −0.29
13	decay rates		−4.08 0 2.38	−4.03 −0.29 2.32
14		$\omega_{\text{decay }[k]}/\omega_{\text{decay pend}}$	{13.10, 1, 2.32}	{13.10, 1.06, 2.26}
15	Constrained	$\{v_{P\{1\}}\}_{\mathbf{x}}/v_P$	{0.001364, 0.001508, 0.001364}	{0.001383, 0.001506, 0.001339}
16	velocity	$\{v_{P\{2\}}\}_{\mathbf{x}}/v_P$	{1.0, 0, −1.0}	{1.04379, −0.00807, −0.77165}
17	components	$\{v_{P\{3\}}\}_{\mathbf{x}}/v_P$	{0.439984, −0.024116, 0.439984}	{0.38002, −0.02458, 0.51840}

would move identically, and the support beams could be reclamped without changing the subsequent motion. A consequence of this is that two of the mode/frequency pairs of the related dissipationless linear system are two-clock versions of those of the one-clock system. In these modes the two pendulums move together in the same phase. Contrastingly, if we start the complete identical clock system with equal and opposite pendulum displacements and velocities and with zero support mass displacement and velocity, then each pendulum would move exactly opposite to the other, and the resultant reaction force and impulse exerted on the support mass would be identically zero. The support mass would remain stationary, and each pendulum would move like the pendulum of a fixed-pivot clock, in opposite phase to the other. This motion corresponds to the intermediate frequency mode/frequency pair. Important (additional three-degree-of-freedom-system) results are that two clocklike mode/frequency pairs now exist and that support mass amplitude for the clocklike, pendulums-in-opposite-phase mode (2) is significantly less than support mass amplitude for the clocklike, pendulums-in-same-phase mode (3), $|y_{(2)}| \ll |y_{(3)}|$.

We can see consequences of this two-clocklike-modes/one-non-clocklike-mode result by thinking about three Fig. 4-like, equal-modal-energy, two-mode-pairings. The $\mathbf{x}_{(1)}, \mathbf{x}_{(3)}$ and $\mathbf{x}_{(1)}, \mathbf{x}_{(2)}$ pairings (projected on an $(\dot{x}_1, \dot{y})$ plane) would show bounding parallelograms with significantly longer sides parallel to the clocklike modal vectors. These comparisons, therefore, each favor the clocklike mode over the non-clocklike mode. However, the $\mathbf{x}_{(2)}, \mathbf{x}_{(3)}$ pairing (now projected on an $(\dot{x}_1, \dot{x}_3)$ plane) would show a bounding parallelogram with almost equal length sides and would not favor either clocklike mode over the other.

Next, examine the change in velocity vectors. We can understand the numerical results by observing that, because support mass is significantly greater than pendulum mass, firing of escapement 1 (for positive pendulum 1 pre-firing relative velocity) would produce a (normalized) change in velocity vector with $\mathbf{x}$ coordinates that can be approximated by $(1, 0, 0)$, the fixed support result. In the $(\dot{x}_1, \dot{x}_3)$ plane this vector would have approximately equal components along the projections of the clocklike modal vectors, since these projections have approximately equal lengths, are orthogonal to each other, and make equal angles with the $\dot{x}_1$ axis. Row 7 of Table 1 shows that the exact, escapement 1-firing-caused change in velocity vector does indeed have the expected approximately equal magnitude components along the two clocklike modal directions and also has a significantly smaller component along the non-clocklike modal direction. When only escapement 3 fires (row 8) the change in velocity vector has the same three-component magnitudes but has the sign of the $\mathbf{x}_{(2)}$ component reversed. For simultaneous, same-direction escapement firings (row 9) the change in velocity vector is the sum of the individual vectors, and for simultaneous, opposite direction escapement firings (row 10) it is the difference. Three important results emerge. Simultaneous same-direction firings produce a large change in velocity in the clocklike, same-pendulum-phase mode (3), a small change in velocity in the non-clocklike, same-pendulum-phase mode (1), and zero change in velocity in the clocklike, opposite-pendulum-phase mode (2). Simultaneous opposite-direction firings produce a large change in velocity in the clocklike, opposite-pendulum-phase mode (2), and zero change in velocity for the two same-pendulum-phase modes. And the magnitudes of the large changes in modal velocity for the two clocklike modes are approximately equal. We conclude then that simultaneous escapement firings also favor each clocklike mode over the non-clocklike mode, but do not favor one clocklike mode over the other.

Next consider the modal and coupling decay rates of the related damped linear system. As for the one-clock system, the modal damping of the clocklike, high-frequency mode is significantly less than that of the non-clocklike, low-frequency mode. Now, in addition, we see that the modal damping of the clocklike, intermediate frequency mode is significantly less than that of the clocklike, high-frequency mode. The basic reason for this is that the relatively high support friction dissipates more energy in the greater-support-velocity-amplitude, high-frequency mode. So we see that the analysis of the related damped linear system not only favors each clocklike mode over the non-clocklike mode, but also favors the clocklike, pendulums-in-opposite-phase mode over the clocklike, pendulums-in-same-phase mode. Additionally, note that because of the symmetries of this identical clock system, there is no linear coupling between the two same-phase modes and the opposite-phase mode—the off-diagonal elements in the second row and column of the $\omega_{\text{decay}\,(i,j)}$ matrix are all zero.

Finally, consider the related modally constrained single-degree-of-freedom systems. First note that two independent linear constraints are required to reduce the three-degree-of-freedom system to a modally constrained single-degree-of-freedom system. For example, to constrain the system to move with coordinates varying in proportion to those of the clocklike, pendulums-in-same-phase mode, one constraint might be a pin pressed into the extended centerline of pendulum 1 a distance above its pivot of $d_{(3)} \equiv (|y_{(3)}|/x_{1(3)}) \cdot e$ sliding in a frictionless vertical slot, and the other a same direction timing belt running over equal diameter massless timing pulleys that rotate with the pendulums. We observe that the constrained, steady-state pendulum velocity amplitudes corresponding to the clocklike, pendulums-in-opposite-phase mode are significantly greater than those corresponding to the clocklike, pendulums-in-same-phase mode. Again we see the system favoring the pendulums-in-opposite-phase clocklike mode over the pendulums-in-same-phase one. And the basic reason is the same—in the favored mode the high friction support mass does not move, so that the escapement supplied energy only gets dissipated in the pendulum dampers.

This clear favoring of the clocklike, pendulums-in-opposite-phase mode leads us to predict that for virtually all initial conditions, the pendulums of the idealized system would synchronize and move in the synchronized steady state with a motion that is accurately approximated by that of the favored modally constrained single-degree-of-freedom system. Here, because of the symmetries of the identical clock system, we can even do a little better. If the system were started with arbitrary, but equal and opposite pendulum displacements and velocities and zero support mass displacement and velocity, an exact solution of the system equations is possible. The system would run the way two identical, fixed-pivot clocks simultaneously started in opposite directions would. This would happen because the linear coupling between the opposite-phase mode and each of the two same-phase modes is zero (rows 11–13) and because simultaneous opposite direction escapement firings cause zero changes in the same-pendulum-phase modal velocities (row 10). Similarly, if the system were started with arbitrary, but equal pendulum displacements and velocities and arbitrary support mass displacement and velocity, an exact numerical solution of the system equations is possible. In the steady state the system would run in a pendulums-in-same-phase version of the calculated motion shown in Fig. 6. From the results of the analyses we also expect, that if we developed numerical techniques for accurately handling non-simultaneous escapement firings, we would find the favored, pendulums-in-opposite-phase steady-state motion to be stable with respect to small departures in initial conditions, and the pendulums-in-same-phase steady-state motion to be unstable.

Now consider the different clock manifestation. The basic results and predictions are the same as for the identical-clock manifestation. Thus, there are two clocklike modes and one non-clocklike mode. In one clocklike mode, the high-frequency mode, the pendulums move in the same phase and in the other, the intermediate frequency mode, the pendulums move in the opposite phase. Simultaneous same-direction escapement firings produce a large velocity change in the clocklike, pendulums moving-in-same-phase mode, and significantly smaller velocity changes in the other two modes; simultaneous opposite-direction escapement firings produce a large velocity change in the clocklike, pendulums-moving-in-opposite-phase mode, and significantly smaller velocity changes in the other two modes; and the magnitudes of these large velocity changes are not too different. The modal decay rate of the clocklike, pendulums-moving-in-opposite-phase mode is significantly less than that of the clocklike, pendulums-moving-in-same-phase mode. The constrained single-degree-of-freedom system corresponding to the clocklike, pendulums-moving-in-opposite-phase mode has a significantly greater mean pendulum velocity amplitude than does the constrained system corresponding to the clocklike, pendulums-moving-in-same-phase mode. We therefore predict that the different clock idealized system will also synchronize, with a synchronized steady-state motion that is accurately approximated by the steady-state motion of the modally constrained, clocklike, pendulums-moving-in-opposite-phase mode, single-degree-of-freedom system. Note that the small asymmetries in going to the different-clock system, while only reducing mean constrained pendulum velocity amplitude from 1.0 to about 0.908, have reduced pendulum 3's amplitude significantly more, to about 0.772. The writer guesses that this amplitude is significantly above a restart threshold of a modified model that includes threshold friction and finite escapement limits.

Before using this three-degree-of-freedom model to examine when no synchronization at all might be predicted (in Section 7), a model that also includes the suspended clock-case feature of Huygens' setup is analyzed.

6. Two-coupled-clock, sliding-support, suspended-clock-case, five-degree-of-freedom model

6.1. Model and equations

Fig. 1 shows the two-coupled-clock, sliding-support, suspended-clock-case, five-degree-of-freedom model. The coordinate vector is now defined as $\mathbf{x} \equiv \{x_1, u_2, y, u_4, x_5\}$, where the x_i, $i = 1, 5$ now denote the horizontal relative displacements of the pendulum mass centers measured from the centerlines of the pivoted clock cases, the u_j, $j = 2, 4$ denote the horizontal relative displacements of the clock-case mass centers measured from vertical lines drawn on the support mass, and y still denotes the absolute horizontal displacement of the support mass (this coordinate ordering again reflects the connectivity of the rigid bodies that comprise the model).

Twelve additional parameters describe this pivoted-case model: the individual clock-case masses, m_j; the individual clock-case lengths, e_j; the individual squares of ratios of radii of gyration about mass centers to lengths, α_j; the individual pivot damping constants, $c_{\text{pivot}\,j}$; the individual air damping constants, $c_{\text{air}\,j}$; and the individual offsets of the pendulum pivots (the downward distances along the clock-case centerlines from the clock-case pivots to the pivots of the pendulums), o_j; $j = 2, 4$. As with the individual clock parameters, it is convenient to introduce

redundant average and half-difference clock-case parameters, using definitions like, $m_{\text{case}} \equiv (m_2 + m_4)/2$ and $\varepsilon_{\text{case}\,m} \equiv (m_2 - m_4)/(2m_{\text{case}})$. The matrices and the impulse forcing vector for this system can then be written as

$$\mathbf{M}_x \equiv \frac{1}{m(1+\alpha)} \begin{bmatrix} m_{11} & m_{12} & m_1 & 0 & 0 \\ m_{12} & m_{22} & m_{23} & 0 & 0 \\ m_1 & m_{23} & m_{33} & m_{43} & m_5 \\ 0 & 0 & m_{43} & m_{44} & m_{54} \\ 0 & 0 & m_5 & m_{54} & m_{55} \end{bmatrix}, \quad \mathbf{K}_x \equiv \frac{1}{mg/e} \begin{bmatrix} k_{11} & k_{12} & 0 & 0 & 0 \\ k_{12} & k_{22} & 0 & 0 & 0 \\ 0 & 0 & 2k_{\text{sup}} & 0 & 0 \\ 0 & 0 & 0 & k_{44} & k_{54} \\ 0 & 0 & 0 & k_{54} & k_{55} \end{bmatrix},$$

$$\mathbf{C}_x \equiv \frac{1}{c_{\text{pivot}} + c_{\text{air}}} \begin{bmatrix} c_{11} & c_{12} & c_{\text{air}\,1} & 0 & 0 \\ c_{12} & c_{22} & c_{23} & 0 & 0 \\ c_{\text{air}\,1} & c_{23} & c_{33} & c_{43} & c_{\text{air}\,5} \\ 0 & 0 & c_{43} & c_{44} & c_{54} \\ 0 & 0 & c_{\text{air}\,5} & c_{54} & c_{55} \end{bmatrix}, \quad \{\mathbf{q}_x\} \equiv \frac{1}{I} \begin{Bmatrix} I_1 \operatorname{sign}(\dot{x}^-_{1,j+1}) \\ 0 \\ 0 \\ 0 \\ I_5 \operatorname{sign}(\dot{x}^-_{5,j+1}) \end{Bmatrix}, \tag{16}$$

with the additional matrix elements defined as

$$m_{ii} \equiv m_i(1+\alpha_i), \quad i = 1,5, \quad m_{ij} \equiv m_i\left(\frac{o_j + e_i}{e_j} + \alpha_i \frac{e_i}{e_j}\right), \quad i,j = 1,2 \text{ or } 5,4,$$

$$m_{jj} \equiv m_j(1+\alpha_j) + m_i\left(\frac{o_j + e_i}{e_j}\right)^2 + m_i\alpha_i \frac{e_i}{e_j}, \quad i,j = 1,2 \text{ or } 5,4,$$

$$m_{j3} \equiv m_i\left(\frac{o_j + e_i}{e_j}\right) + m_j, \quad i,j = 1,2 \text{ or } 5,4, \quad m_{33} \equiv m_1 + m_2 + 2m_{\text{sup}} + m_4 + m_5,$$

$$k_{ii} \equiv m_i g/e_i, \quad i = 1,5, \quad k_{ij} \equiv m_i g/e_j, \quad i,j = 1,2 \text{ or } 5,4,$$

$$k_{jj} \equiv \left(\frac{m_i g}{e_j}\right)\left(\frac{o_j + e_i}{e_j}\right) + \left(\frac{m_j g}{e_j}\right), \quad i,j = 1,2 \text{ or } 5,4,$$

$$c_{ii} \equiv c_{\text{pivot}\,i} + c_{\text{air}\,i}, \quad i = 1,5, \quad c_{ij} \equiv c_{\text{air}\,i}\left(\frac{o_j + e_i}{e_j}\right), \quad i,j = 1,2 \text{ or } 5,4,$$

$$c_{jj} \equiv c_{\text{air}\,i}\left(\frac{o_j + e_i}{e_j}\right)^2 + c_{\text{pivot}\,j} + c_{\text{air}\,j}, \quad i,j = 1,2 \text{ or } 5,4,$$

$$c_{j3} \equiv c_{\text{air}\,j} + c_{\text{air}\,i}\left(\frac{o_j + e_i}{e_j}\right), \quad i,j = 1,2 \text{ or } 5,4; \quad c_{33} \equiv c_{\text{air}\,1} + c_{\text{air}\,2} + 2c_{\text{sup}} + c_{\text{air}\,4} + c_{\text{air}\,5}, \tag{17}$$

and, as for the previous model, if only escapement 1 fires, I_5 is to be set to zero; if only escapement 5 fires, I_1 is to be set to zero; and if both escapements fire simultaneously, the impulse forcing vector is to be used as written.

6.2. Setting parameter values

Even less information is available to use for estimating the actual values of the clock-case parameters of Huygens' setup [4] than for the clock parameters. But, as has been seen for the previous models, as long as basic properties of the system are captured, useful results can be obtained. In this spirit, and making educated guesses as to Huygens' design constraints and goals, new parameters are defined and their values set and some old parameters are redefined and/or their values reset:

$$\mu_{\text{case}} \equiv m_{\text{case}}/m = 85, \quad \alpha_{\text{case}} = 0.4, \quad \mu = 25, \quad o_{\text{case}} = 1.0 \cdot e,$$

$$\omega_{\text{n case}} \equiv \sqrt{\frac{m_{\text{case}} g/e_{\text{case}}}{m_{\text{case}}(1+\alpha_{\text{case}})}} = 0.5\omega_{\text{n pend}},$$

$$\omega_{\text{n sup}} \equiv \sqrt{2k_{\text{sup}}/(2m + 2m_{\text{case}} + 2m_{\text{sup}})} = 0.4\omega_{\text{n pend}},$$

$$\omega_{\text{decay case}} \equiv \frac{c_{\text{pivot case}} + c_{\text{air case}}}{2m_{\text{case}}(1+\alpha_{\text{case}})} = 10\omega_{\text{decay pend}},$$

$$\omega_{\text{decay sup}} \equiv \frac{2c_{\text{air}} + 2c_{\text{air case}} + 2c_{\text{sup}}}{2(2m + 2m_{\text{case}} + 2m_{\text{sup}})} = 14\omega_{\text{decay pend}},$$

$$f_{\text{air case}} \equiv c_{\text{air case}}/(c_{\text{air case}} + c_{\text{pivot case}}) = 0.5. \tag{18}$$

Some reasons for these choices follow. The high value chosen for m_{case} reflects Huygens having made the extended clock-cases as massive as practicable in order to keep the clock-cases near vertical on a rocking ship. The reduction in μ reflects the writer having increased support mass over his best guess for the previous, translating-clock-case model, to include effects of equivalent translating clock-case mass there. The choice for α_{case} reflects the extended clock-case masses being spread out considerably farther around their mass centers than the pendulum masses are around theirs. The inertia parameter choices for this model then reflect the basic system features that the extended clock-case masses and half the support mass are each considerably greater than mean pendulum mass, with mean extended-clock-case mass also being significantly greater than half the support mass.

The choice of the relatively small value for o_{case} reflects the writer's belief that Huygens would have made the offsets as small as practicable so as to impart as little horizontal clock-case relative motion to the pendulums as possible. The value chosen for $\omega_{\text{n case}}$ reflects the writer's guess that Huygens designed to a spatial constraint that clock-case length be at most about four times pendulum length. The value chosen for $\omega_{\text{n sup}}$ is arbitrary; it has been guessed, with virtually no information, to be a 'most likely' value; and its value is close enough to that of $\omega_{\text{n case}}$ to also

explore whether some 'resonant interaction' between these two frequencies significantly affects the clocklike mode shapes of the related dissipationless linear system (no obvious effects were found).

The choices of the decay friction parameter values reflect the judgment that both case and support friction, while small, were still significantly greater than pendulum friction, which was extremely small. These choices also reflect the judgment that support friction, which was mostly chair-back friction, was greater than clock-case friction. The choice of an equal division of clock-case friction between its pivot- and air-friction parts, like the previously assumed division of pendulum friction between these parts, is arbitrary. These choices reflect the judgment that relatively large changes in these parameter values will have negligible effects on the basic results.

6.3. Identical clock/clock-case results

Although it is unlikely that Huygens' extended clock-cases were near being identical, it is instructive to analyze an identical-clock, identical-clock-case model. Results of this analysis are shown in the 'Identical Clocks and Clock-Cases' column of Table 2. Two clocklike mode/frequency pairs also exist for this model. In the clocklike, pendulums-in-opposite-phase mode (4) each clock case moves opposite to its pendulum, and, because of system symmetries, the support mass does not move. Contrastingly, in the clocklike, pendulums-in-same-phase mode (5) each clock case moves in-phase with its pendulum, and the support mass moves in-opposite-phase to the other four masses. Results for mode (3), which has the greatest modal pendulum amplitudes of the three non-clocklike modes, are also shown. In mode (3) the two clock-cases move in-phase with each other against (in opposite-phase with) the two pendulums and the support mass. So, on the basis of relative pendulum amplitudes, each clocklike mode is clearly favored over each of the three non-clocklike modes. However, the small pendulum-amplitude advantage of clocklike mode (4) over clocklike mode (5), would not, by itself, lead most observers to conclude that mode (4) is clearly favored over mode (5). So, again, analysis of the related dissipationless linear system favors the clocklike modes over the non-clocklike ones but does not immediately (not looking ahead to the analyses of the related damped linear system) favor one clocklike mode over the other.

The related dissipationless nonlinear system also favors the clocklike modes over the non-clocklike modes and does not clearly favor one clocklike mode over the other. Individual escapement firings cause relatively large and approximately equal modal velocity changes in the clocklike modes and significantly smaller modal velocity changes in the non-clocklike modes. As with the three-degree-of-freedom model, this then leads to simultaneous same direction escapement firings favoring the clocklike, pendulums-in-same-phase mode and to simultaneous opposite direction escapement firings favoring the clocklike, pendulums-in-opposite-phase mode, with no decisive advantage of one over the other.

Analyzing the related damped linear system shows that the pendulums-in-opposite-phase clocklike mode [4] has a significantly lower decay rate than the corresponding pendulums-in-same-phase clocklike mode [5]. Part of this favoring occurs as for the three-degree-of-freedom model, because the relatively heavily damped support mass moves through lower amplitudes in the favored damped mode. But an additional part occurs because the relatively heavily damped clock cases now also move through lower amplitudes in the favored damped mode.

Table 2
Comparing two, five-degree-of-freedom, two-clock, suspended-clock-case, sliding-support models

Row	Item	Symbol	Identical clocks and clock cases	Clock 1 and clock-case 4 sluggish
1	Natural frequency,	$\omega_{n\,(3)}/\omega_{\text{n pend}}$,	0.886,	0.884,
2	modal vector	$\mathbf{x}_{(3)}$	$\{0.314, -0.126, 0.118, -0.126, 0.314\}$	$\{0.304, -0.138, 0.118, -0.116, 0.304\}$
3		$\omega_{n\,(4)}/\omega_{\text{n pend}}$,	1.001,	0.999,
4		$\mathbf{x}_{(4)}$	$\{1.002, -0.004, 0, 0.004, -1.002\}$	$\{1.218, 0.005, -0.011, 0.012, -0.714\}$
5		$\omega_{n\,(5)}/\omega_{\text{n pend}}$,	1.018,	1.019,
6		$\mathbf{x}_{(5)}$	$\{0.954, 0.043, -0.049, 0.043, 0.954\}$	$\{0.656, 0.043, -0.046, 0.038, 1.191\}$
7	Change in	$\Delta\dot{\mathbf{w}}_{j+1\text{ esc 1 only}}/\Delta v$	$\{0.002, 0.015, 0.222, 0.708, 0.675\}$	$\{0.001, 0.014, 0.189, 0.758, 0.408\}$
8	velocity vectors	$\Delta\dot{\mathbf{w}}_{j+1\text{ esc 5 only}}/\Delta v$	$\{0.002, -0.015, 0.222, -0.708, 0.675\}$	$\{0.003, -0.017, 0.241, -0.565, 0.943\}$
9		$\Delta\dot{\mathbf{w}}_{j+1\text{ same dir}}/\Delta v$	$\{0.004, 0, 0.444, 0, 1.349\}$	$\{0.004, -0.004, 0.430, 0.193, 1.352\}$
10		$\Delta\dot{\mathbf{w}}_{j+1\text{ opp dir}}/\Delta v$	$\{0, 0.030, 0, 1.417, 0\}$	$\{-0.002, 0.031, 0.052, 1.323, 0.535\}$
11	Modal and		$\vdots\ \vdots\ \vdots\ \vdots$	$\vdots\ \vdots\ \vdots\ \vdots$
12	coupling	$\omega_{\text{decay }(i,j)}/\omega_{\text{decay pend}}$	$\cdots\ 22.69\ \ 0\ \ -8.37$	$\cdots\ 22.89\ \ 1.80\ \ -7.92$
13	decay rates		$\cdots\ 0\ \ 1.019\ \ 0$	$\cdots\ 1.80\ \ 1.223\ \ -0.75$
14			$\cdots\ -8.37\ \ 0\ \ 4.314$	$\cdots\ -7.92\ \ -0.75\ \ 3.902$
15		$\omega_{\text{decay }[k]}/\omega_{\text{decay pend}}$	$\{10.61, 9.98, 24.22, 1.018, 2.756\}$	$\{10.41, 10.63, 24.30, 1.228, 2.462\}$
16	Constrained	$\{v_{P\{3\}}\}_{\mathbf{x}}/v_P$	$\{0.005, -0.002, 0.002, -0.002, 0.005\}$	$\{0.004, -0.002, 0.002, -0.002, 0.004\}$
17	velocity	$\{v_{P\{4\}}\}_{\mathbf{x}}/v_P$	$\{0.986, -0.004, 0, 0.004, -0.986\}$	$\{0.933, 0.004, -0.009, 0.009, -0.547\}$
18	components	$\{v_{P\{5\}}\}_{\mathbf{x}}/v_P$	$\{0.220, 0.010, -0.011, 0.010, 0.220\}$	$\{0.167, 0.011, -0.012, 0.010, 0.304\}$

The analyses of the related modally constrained nonlinear systems then show that, primarily because of the difference in modal decay rates, steady-state pendulum velocity amplitudes are significantly greater for the clocklike, modally constrained, pendulums-in-opposite-phase motions than for the corresponding same-phase motions. Thus, the analyses guide us to predict that the idealized identical clocks will again synchronize, all mass points moving nearly proportionally and the pendulums moving in opposite-phase. Note that this symmetric five-degree-of-freedom system cannot achieve the ideal, pendulum-only-dissipation of the fixed pivot clock—even though the support mass remains motionless in the favored pendulums-in-opposite-phase modal motion, the clock-cases still must move against their relatively high friction dampers. However, the high ratio of clock-case mass to pendulum mass makes these clock-case amplitudes small, so that mean pendulum velocity amplitude is only reduced to about 0.986 times the ideal amplitude.

6.4. Non-identical clock/clock-case results

Half difference parameters are chosen for the non-identical clock/clock-case model as follows. First, the clock half difference parameters are made the same as those of the three-degree-of-freedom model. Then, observing from a sketch in Huygens' laboratory notebook [4] that Huygens seemed to be trying to determine how heavy the extended clock cases needed to be by adding significant extra mass to the bottom of one clock case, and noting that there were no particular reasons for Huygens to try making the clock-cases identical, the following arbitrary half difference clock-case parameters were chosen (all in the direction that would make clock-case 4 more sluggish): $\varepsilon_{\text{case m}} = -0.20$; $\varepsilon_{\text{case }\alpha} = -0.08$; $\varepsilon_{\text{case e}} = -0.10$; $\varepsilon_{\text{case }c_{\text{pivot}}} = -0.08$; $\varepsilon_{\text{case }c_{\text{air}}} = -0.08$; $\varepsilon_{\text{case o}} = -0.06$.[2]

Results of the analyses of this non-identical clock/clock-case model are shown in the last column of Table 2. The basic result is that the asymmetric, five-degree-of-freedom system is predicted to behave essentially as the symmetric (identical-clock/clock-case) one does—the clocks will synchronize, with the pendulums moving nearly proportionally in the clocklike, pendulums-in-opposite-phase mode of the related dissipationless linear system. The key results are that: although the modal decay rate ratio changes from about $1.018/2.756 \approx 0.37$ to $1.228/2.462 \approx 0.51$ in going from the symmetric- to the asymmetric-configuration, the modal decay rate ratio still significantly favors the pendulums-in-opposite-phase mode over the pendulums-in-same-phase mode; and, although the constrained steady-state pendulum-mean-velocity-amplitude ratio changes from about $0.986/0.220 \approx 4.48$ to about $0.740/0.236 \approx 3.14$ in going from the symmetric- to the assymmetric-configuration, the pendulum-mean-velocity-amplitude ratio still significantly favors the pendulums-in-opposite-phase mode over the pendulums-in-same-phase mode. Note that going to the assymmetric configuration causes additional decreases in constrained pendulum velocity amplitudes from the ideal: the change due to allowing the clock-cases to pivot reduces (both) pendulum velocity amplitudes to 0.986 times the ideal; also allowing assymmetries further reduces the mean pendulum velocity amplitude to 0.740 times the ideal and that of pendulum 5 to 0.547 times the ideal (a value the writer guesses is still significantly above a restart threshold for a model with realistically modeled threshold friction and escapement limits).

[2]Offsets, o_j, appear in numerator terms of the diagonal elements of the even rows of the inertia and damping matrices, so the writer has guessed that a negative sign here will also tend to make clock-case 4 more sluggish.

So we see that allowing the clock-cases to pivot and allowing relatively large assymmetries still gives systems that are predicted to synchronize, even though predicted constrained pendulum velocity amplitudes depart significantly from those of fixed pivot clocks.

7. Predicting absence of synchronization and speculations

7.1. Predicting absence of synchronization

First observe that a necessary condition for synchronization to be predicted is that one modal decay rate be significantly less than all others. This suggests a way to modify models of Huygens' setup so that the absence of synchronization will be predicted. Take the three-degree-of-freedom models of Section 5 and, while keeping all other parameters constant, increase support mass by a factor of 14, the (former) value of f_{decay}, the ratio of support decay rate to pendulum decay rate (see Eq. (10)). We also see that, since support mass dominates the denominator of the definition of $\omega_{\text{decay sup}}$, this change reduces support decay rate so that it becomes about equal to pendulum decay rate. This near equality of constrained decay rates, in turn, makes all three modal decay rates approximately equal, preventing one damped mode from persisting after all others have decayed. (Incidentally note that, because support mass was originally much greater than pendulum mass, this further increase does not significantly change the basic features of the clocklike mode/frequency pairs.)

Analysis results are listed in Table 3. We see by comparing the modal decay rates and constrained velocity amplitude components of the identical clock models of Tables 1 and 3 that increasing support mass has wiped out the advantages of the clocklike, pendulums-in-opposite-phase mode over the clocklike, pendulums-in-same-phase mode. For the original support mass value the modal decay rate ratio was $1/2.32 \approx 0.43 \ll 1$, and the pendulum velocity amplitude ratio was $1/0.440 \approx 2.27 \gg 1$, while with the increase in support mass these ratios have become $1.0/1.002 \approx 0.998 \not\ll 1$ and $1.0/1.00099 \approx 0.999 \not\gg 1$. Because the modal decay rates have become approximately equal, the clocklike, pendulums-in-opposite-phase mode of the related damped linear system would not persist after the clocklike, pendulums-in-same-phase mode had decayed. Both clocklike modes would decay at approximately the same rate; neither is favored over the other; and we would predict that synchronization is unlikely to occur.

The modal decay rate comparison behaves similarly for the different-clock model. Increasing support mass changes the modal decay rate ratio from $1.06/2.26 \approx 0.47 \ll 1$ to $1.075/0.926 \approx 1.16 \not\ll 1$, so that again, neither clocklike mode is significantly favored over the other by friction alone. However, the modally constrained mean pendulum velocity amplitude comparison might be judged to favor one clocklike mode over the other, and a clear prediction of synchronization or no-synchronization does not follow from the approximate analyses. The mean pendulum velocity amplitude ratio changes from $0.908/0.449 \approx 2.02 \gg 1$ to $0.463/0.677 \approx 0.68 \not\gg 1$, and so, since $1/0.68 \approx 1.46$ might be judged to be significantly greater than one, this comparison now seems to favor the constrained, clocklike, pendulums-in-same-phase mode {3} over the constrained, clocklike, pendulums-in-opposite-phase mode {2}. However, the constrained mode {3} velocity amplitude of pendulum 1 is only about 0.079, a value that the writer guesses would not significantly exceed a restart threshold. So the writer thinks it is unlikely that the corresponding

Table 3
Non-synchronizing, three-degree-of-freedom, two-clock, sliding-pivot models

Row	Item	Symbol	Identical clocks	Clock 1 sluggish
1	Natural frequency,	$\omega_{n\,(1)}/\omega_{\text{n pend}}$,	0.189684,	0.189684,
2	modal vector	$\mathbf{x}_{(1)}$	{0.00173, 0.04670, 0.00173}	{0.00174, 0.04670, 0.00171}
3		$\omega_{n\,(2)}/\omega_{\text{n pend}}$,	1.0,	0.996052,
4		$\mathbf{x}_{(2)}$	{1.0, 0, −1.0}	{1.40874, −0.00149, −0.08638}
5		$\omega_{n\,(3)}/\omega_{\text{n pend}}$,	1.001111,	1.005112,
6		$\mathbf{x}_{(3)}$	{1.00107, −0.00224, 1.00107}	{0.08745, −0.00168, 1.41588}
7	Change in	$\Delta\dot{\mathbf{w}}_{j+1\text{ esc 1 only}}/\Delta v$	{0.00122, 0.70711, 0.70786}	{0.00108, 0.87659, 0.05442}
8	velocity vectors	$\Delta\dot{\mathbf{w}}_{j+1\text{ esc 3 only}}/\Delta v$	{0.00122, −0.70711, 0.70786}	{0.00136, −0.06841, 1.12132}
9		$\Delta\dot{\mathbf{w}}_{j+1\text{ same dir}}/\Delta v$	{0.00244, 0, 1.41573}	{0.00244, 0.80819, 1.17574}
10		$\Delta\dot{\mathbf{w}}_{j+1\text{ opp dir}}/\Delta v$	{0, 1.41421, 0}	{−0.00027, 0.94500, −1.06690}
11	Modal and		1.028 0 −0.024	1.028 −0.015 −0.019
12	coupling	$\omega_{\text{decay }(i,j)}/\omega_{\text{decay pend}}$	0 1.0 0	−0.015 1.075 0.010
13	decay rates		−0.024 0 1.002	−0.019 0.010 0.926
14		$\omega_{\text{decay }[k]}/\omega_{\text{decay pend}}$	{1.028, 1.0, 1.002}	{1.028, 1.075, 0.926}
15	Constrained	$\{v_{P\{1\}}\}_{\mathbf{x}}/v_P$	{0.000001, 0.000015, 0.000001}	{0.000001, 0.000015, 0.000001}
16	velocity	$\{v_{P\{2\}}\}_{\mathbf{x}}/v_P$	{1.0, 0.0, −1.0}	{0.87270, −0.00092, −0.05351}
17	components	$\{v_{P\{3\}}\}_{\mathbf{x}}/v_P$	{1.00099, −0.00224, 1.00099}	{0.07883, −0.00151, 1.27628}

system with realistically modeled threshold friction and escapement limits would actually develop a stable synchronized steady-state motion (more detailed speculations follow).

7.2. Speculations

The writer believes that, for suitably chosen initial conditions, the behaviors of the idealized models analyzed herein would accurately reflect the behaviors of the real systems they model. As noted, however, idealized- and real-model behaviors are expected to differ significantly when initial conditions and parameters are such that a pendulum passes through a low-energy (low displacement- and velocity-magnitude) cycle. For real systems (for models that include threshold friction and small, but finite, displacement-interval and velocity-magnitude firing requirements on the escapements), the expected behavior is for a pendulum to stop during its first low energy cycle.

To ensure starting, consider behaviors of example real systems having high-energy initial conditions. First, consider the real system corresponding to the different clock model of Table 1, started with initial displacements of zero and initial velocities equal to $2\omega_{\text{n pend}}\mathbf{x}_{(2)}$. Almost all initial energy of this system (four times the reference energy corresponding to each scaled, normalized, undamped modal vector) would be in the intermediate-frequency damped normal mode [2], with small amounts in the other two. The trajectory projection on the $(\dot{x}_1, \dot{x}_3)$ plane would be near an escapement-firing-boosted, slowly decaying, narrow spiral, centered about a line in the intermediate-frequency modal direction (resembling a combination of Figs. 5 and 6, with four escapement-firing-boosts per cycle instead of two). Zero pendulum displacements would occur nearly simultaneously with opposite direction velocities, and the corresponding, nearly simultaneous escapement firings would, therefore, tend to put most of the supplied energy into the intermediate frequency mode [2]. The system would be expected to slowly approach (over a large number of pendulum cycles, as illustrated by the transient trajectory of Fig. 3) a steady-state that has the features of the steady-state motion of the related constrained nonlinear system {2} (the steady-state trajectory projection would be like that of Fig. 6, except that there would be a neighboring pair of small, escapement-firing-caused velocity changes replacing each small simultaneous-escapement-firing-caused change). An observer would see the two pendulums oscillating at about the constrained pendulum frequency, $\omega_{\text{n pend}}$, moving approximately in-opposite-phase to each other, with slowly decreasing amplitudes that remain in the ratio of the pendulum amplitude components of the modal vector and that approach the amplitudes predicted for the related, modally constrained single-degree-of-freedom system {2}. No small pendulum amplitude cycles would occur during this approach to a steady state, so the writer expects that for these initial conditions the real system would synchronize.

Next, consider the same (real) system, now started with similar, equal-energy initial conditions that correspond to the high-frequency clocklike mode (3). The writer guesses that the resulting motion would occur in two recognizably different stages. First, over a relatively large number of pendulum cycles, the system would behave analogously to its previous behavior, modified now by having a higher rate of decay and by the escapements firing (still nearly simultaneously) in the same, rather than opposite, directions. During this stage the amplitudes would slowly decay to some values between the starting amplitudes and the calculated amplitudes for the related, modally constrained single-degree-of-freedom system {3}. The writer guesses that amplitudes would stabilize before the difference between the clocklike modal decay rates causes the

escapement firings to move significantly from being nearly simultaneous and in the same direction. Then, once amplitudes stabilize, the second recognizable stage would begin. This stage would involve a slow change in the proportions of system energy in each clocklike mode. Energy fraction in the favored clocklike mode [2] would slowly increase. During the slow increase, the two escapements would have to gradually change from nearly simultaneous same direction firings to nearly simultaneous opposite direction firings.

To clarify what could happen during such a slow transition, consider an idealized, simplified half-way situation, formed by restarting the system with equal energies in each of the two undamped clocklike modes. The initial displacements would again be zero, but the initial velocities would be $a\omega_{\text{n pend}} \cdot (\mathbf{x}_{(2)} \mapsto +\mathbf{x}_{(3)})$, where the scalar, a, would be high enough so that both pendulums would move through at least one cycle. The 'bounding' parallelogram (analogous to that of Fig. 4) would now be approximate, as its modal components would be narrow spirals rather than lines. It would have sides that shrink exponentially at different rates, that are initially approximately equal in length, and that are approximately orthogonal to each other. Additionally, because the component oscillations are both clocklike, their frequencies, while distinct, would be approximately equal. Thus, temporarily ignoring effects of escapement firings, we see that beating could occur—the almost same frequency pendulum oscillations could change, over many cycles, from being approximately in the same phase, to being approximately one-quarter cycle out of phase, to being approximately in opposite phase, etc., until the energy in the more heavily damped mode becomes negligible. Starting at the corner of the sum diagonal of the initially nearly square parallelogram, the trajectory generating point would oscillate at a frequency near $\omega_{\text{n pend}}$, initially tracing a path that lies in the neighborhood of this diagonal. After many pendulum oscillation cycles (about $\omega_{\text{n pend}}/[4(\omega_{\text{nd [3]}} - \omega_{\text{nd [2]}})]$) this point would trace a path that lies in the neighborhood of the ellipse inscribed in the suitably shrunken parallelogram. And then, after about the same additional number of cycles, the path would lie in the neighborhood of the difference diagonal of the further shrunken parallelogram. If, during the shrinking of the parallelogram, one of its diagonals should fall close to one of the coordinate axes while the trajectory generating point is moving in the neighborhood of this diagonal, then the cyclic velocity and displacement amplitudes of the pendulum corresponding to the other coordinate axis would be low, and that real pendulum would stop moving.

It would take a large number of pendulum oscillation cycles for this system to change from near resonant motion in its same-phase clocklike mode [3] to near resonant motion in its opposite-phase clocklike mode [2]. The writer expects that during this long interval, conditions would arise with the trajectory generating point moving in the neighborhood of a diagonal that lies near one of the coordinate axes. This means that most of the system energy would be associated with one pendulum, and the other pendulum would go through a low-energy cycle and stop moving. Thus, the writer concludes that when the possibility of synchronization is predicted and compatible initial conditions are applied, real clocks would indeed synchronize. If initial conditions corresponding to the non-favored clocklike mode are applied, the writer expects a temporary, but ultimately unstable synchronization to occur. The writer expects that eventually the system would try to change to the favored clocklike mode and that during this slow change one of the pendulums would stop moving.

The behaviors of the real systems corresponding to the models of Table 3 are even more uncertain. Because of the extremely large support mass value, changes between clocklike resonant

modes would take significantly more pendulum cycles than corresponding changes for the models of Table 1. Additionally, because neither clocklike mode is significantly favored over the other, any small differential-friction- or differential-escapement-firing-caused changes between modes would tend to take many more pendulum oscillation cycles. Thus, the writer guesses that if the real system corresponding to the identical clock model of Table 3 were started with high-energy modal initial conditions corresponding to either clocklike mode, the system would initially slowly approach the steady-state motion of the appropriate related constrained nonlinear system, but that eventually one or the other pendulums would stop.

Because the clocklike modal vectors of the different-clock model of Table 3 each have one low pendulum amplitude, the writer expects the real, different-clock system to behave differently, stopping after fewer pendulum cycles. The writer expects that when started with high modal energy initial conditions, the real different-clock system would continue to move approximately in that mode until the amplitude of the low-amplitude pendulum gets small enough, and then that pendulum would stop. The writer does not expect the nominal modal steady-state {2 or 3}, to occur before the low-amplitude pendulum stops.

8. Summary

An approximate technique is developed for quantitatively predicting whether two Huygens-like coupled-pendulum-clocks can synchronize. The technique consists of analyzing a sequence of models that are related to nonlinear, multi-degree-of-freedom models of Huygens' setups. These models capture essential features of Huygens' setups—in particular that the escapements impulsively resupply system energy; that the clocks are not identical; and that the extended clock-cases can be suspended from a common support that can move horizontally. The technique is used to predict that Huygens' system would synchronize even if the differences between the clocks drastically exceed the likely differences of Huygens' setups.

References

[1] R. Mirollo, S. Strogatz, Synchronization of pulse-coupled biological oscillators, *SIAM Journal of Applied Mathematics* 50 (6) (1990) 1645–1662.

[2] C. Huygens, Letter to de Sluse in *Oeuveres Complètes de Christiaan Huygens* [referred to as *O.C.* in the references that follow] 5, Correspondance 1664–1665, published for the Société Hollandaise Des Sciences by Martinus Nijhoff, La Haye (1893), Letter No. 1333 of 24 February 1665, 241.

[3] C. Huygens, Attachment to a letter to Constantyn Huygens, his father, in: *O.C.* 5, Letter No. 1335 of 26 February 1665, pp. 243–244.

[4] C. Huygens, *O.C.* 17, *L'Horloge a pendule de 1651 a 1666*, Martinus Nijhoff, La Haye, 1932, pp. 183–187.

[5] C. Huygens, Letter to Moray in *O.C.* 5, Letter No. 1345 of 6 March 1665, pp. 255–256.

[6] C. Huygens, *O.C.* 18, *Horologium Oscillatorium (1673)*, Martinus Nijhoff, La Haye, 1934, pp. 69–368.

[7] C. Huygens, *Christiaan Huygens' The Pendulum Clock or Geometrical Demonstrations Concerning the Motion of Pendula as Applied to Clocks*, Translated by R.J. Blackwell, The Iowa State University Press, Ames, Iowa, 1988.

[8] D.J. Korteweg, *Les Horloges sympathiques de Huygens, les phénomènes connexes et les oscillations principales et composées que présentent deux pendules fixés à un mécanisme à un seul degré de liberté*, in: *Archives Néerlandaises d. Sciences ex. et nat.* Serie II, T. XI, M. Nijhoff, La Haye, 1906, 273–295.

[9] I.I. Blekhman, *Synchronization in Science and Technology*, ASME Press, New York, 1988 (This book is an English translation of *Sinkhronizatsiia v prirode i tekhnike*, Nauka Publishers, Moscow, 1981).
[10] M. Bennett, M.F. Schatz, H. Rockwood, K. Wiesenfeld, Huygens' clocks, *Proceedings Royal Society: A* 458 (2019) (2002) 563–580.
[11] J. Pantaleone, Synchronization of metronomes, *American Journal of Physics* 70 (10) (2002) 992–1000.
[12] A.A. Andronov, A.A. Vitt, S.E. Khaikin, *Theory of Oscillators*, Translated by F. Immirzi, Edited and Abridged by W. Fishwick, Pergamon Press, Oxford, 1966.
[13] E.L. Edwardes, *The Story of the Pendulum Clock*, John Sherratt and Son Ltd., Altrincham, UK, 1977.
[14] A.M. Lepschy, G.A. Mian, U. Viaro, Feedback control in ancient water and mechanical clocks, *IEEE Transactions on Education* 35 (1) (1992) 3–10.
[15] A.V. Roup, D.S. Bernstein, S.G. Nersesov, W.M. Haddad, V. Chellaboina, Limit cycle analysis of the verge and foliot clock escapement using impulsive differential equations and Poincare maps, *International Journal of Control* 76 (17) (2003) 1685–1698.
[16] R.E. Mickens, *An Introduction to Nonlinear Oscillations*, Cambridge University Press, Cambridge, UK, 1981.
[17] S.H. Strogatz, *Nonlinear Dynamics and Chaos*, Addison-Wesley, Reading, MA, 1994.
[18] W.H. Press, S.A. Teukolsky, W.T. Vetterling, B.P. Flannery, *Numerical Recipes in FORTRAN—The Art of Scientific Computing*, second ed., Cambridge University Press, Cambridge, UK, 1992.
[19] T.S. Parker, L.O. Chua, *Practical Numerical Algorithms for Chaotic Systems*, Springer, New York, 1989.